ANDERSON& ASSOCIATES
CONSULTING METALLURGICAL ENGINEERS AND TESTING LABORATORY

~~**PRIVILEGED and CONFIDENTIAL –ATTORNEY-CLIENT WORK PRODUCT**~~

June 13, 2025

South Bow
707 5 Street S.W.
Calgary, AB, Canada, T2P 1V8
Attn: (b)(6)
By Email

Re: 250145 South Bow - Metallurgical Analysis of NPS-30 MP-171 Pipeline Incident

Dear (b)(6)

Pursuant to your request, this report details the findings of the metallurgical investigation of the Keystone Pipeline rupture near MP-171 near Fort Ransom, North Dakota.

NOMENCLATURE and SAMPLE IDENTIFICATIONS

The identification and location of specific features of the pipe are made in reference to top dead center (TDC). Clockwise position is established when viewed in the direction of flow. The locations of individual mechanical test specimens correspond to the specimen identifications. As an example, sample 324-33-9 would indicate 324° clock position, at an axial position of 33ft 9in downstream of girth weld 600 (GW600). A "W" or "H" preceding the clock position indicates "weld centerline" or "heat affected zone", respectively.

Additional Terminology:

Inner Diameter: *ID*
Outer Diameter: *OD*
Upstream: *US*
Downstream: *DS*
Girth Weld: *GW*
Seam Weld: *SW*
Crack Tip Opening Displacement: *CTOD*
Compact Tension: *C(T)*

BACKGROUND INFORMATION

It was reported that at 7:42AM on April 8, 2025, a control center leak detection system identified a pressure drop in the system, triggering a shutdown at 7:44AM. The pipeline was reportedly a 30" nominal diameter with a 0.386" nominal wall thickness, manufactured to be compliant with an API 5L grade X70 PSL 2 material at the Berg Panama City, Florida pipe mill in 2008. The failure was initially reported as having occurred at a seam weld. The material test reports (MTR) for joint is provided as Appendix A and the Manufacturing Procedure Specification and Quality Plan governing the manufacturing of the pipe is included as Appendix B. The failed section of pipe was received at Anderson & Associates on April 17, 2025, and the metallurgical investigation began on April 21, 2025.

Anderson & Associates was retained to perform the metallurgical analysis in accordance with the Mechanical and Metallurgical Testing Protocol for Fort Ransom MP-171 NPS-30 KS6 Incident, as detailed in Appendix C.

ON-SITE EXAMINATION

At the request of the regional director of the Pipeline Hazard Materials Safety Administration (PHMSA), (b)(6) with Anderson & Associates, Inc. was requested to be present at the rupture site near Fort Ransom, North Dakota. The purpose of the on-site presence was to witness the extraction of the ruptured pipe segment and provide consultation to South Bow regarding preservation of the exposed fracture surfaces during transport to Anderson & Associates' laboratory located in Houston, Texas.

Arrival at the rupture location occurred on the morning of April 12 and at that time approximately 100ft of the pipeline had been uncovered/excavated as shown in Figure 1. The feature had been wrapped with cellophane plastic wrap and a traffic cone had been placed between the fractures to allow for the insertion of a suction hose without damaging the exposed fracture surfaces. The focus of efforts at the time of arrival were to insert a stopple plug approximately 150 yards downstream from the rupture location. The plan forward at the time of arrival was to set the stopple, drain the line, and cut out the failed joint. The approximate length of pipe to be removed for analysis was (b)(4) and consisted of the entire length of the ruptured joint, approximately (b)(4) of the upstream joint, and approximately (b)(4 of the downstream joint.

Extraction of the failed joint began in the early morning of April 13, 2025 following the draining of the line. Two, hydraulically powered pipe cold cutting and beveling machines were installed at the pre-determined upstream and downstream cut sites. Cutting of the two ends occurred simultaneously, with the upstream cut completing first and resulted in a slight vertical displacement of the upstream joint. There was no visual deflection of the downstream pipe at the conclusion of the downstream cut. The liberated section of pipe was hoisted out of the ground with the assistance of two excavators lifting in unison to keep the pipe level. The cut ends of the pipe were wrapped with cellophane plastic wrap and capped with pipe covers before being placed on a flat-bed trailer and moved to a location adjacent to the dig site to allow room for the insertion of the replacement joint.

The liberated section of pipe was removed from the flat-bed trailer in the early afternoon of April 13, 2025 and was supported by wood cribbing at a slight angle to allow remnant crude oil to

drain from the pipe. The cellophane wrapping that had initially been placed over the rupture was cut away, allowing the first visual inspection of the rupture which is shown in Figure 2. The rupture appeared as a "fish mouth", and was observed to be partially coincident with the longitudinal seam weld. The fracture was observed to cross a girth weld (GW610) before deflecting in a clockwise direction into the base metal of the downstream joint. The upstream portion of the rupture was also observed to deflect away from the seam weld also in the clockwise direction. It was further noted that the location of top dead center (TDC) on the pipe was marked, the relative clock positions of the seam welds relative to TDC were identified, and the flow direction was also indicated.

Decontamination of the external surface of the pipe around the rupture was performed using Citrol (an all-purpose degreaser) and oil absorbent cloths. Cleaning was performed by authorized personnel wearing appropriate personal protective equipment (PPE). The personnel were instructed to wipe away crude oil from the external surface around the rupture, but to not clean the fracture surfaces. The fracture surfaces were sprayed with WD-40 before being covered with strips of heavy-duty garden hose to protect the fractures during transport. The entire rupture and coverings were then wrapped in poly-wrap and cellophane plastic wrap for transport.

The extracted section of pipe was cut into two approximately equal lengths via circular hydraulic cutter at the (b)(mark for transport and for the purpose of ease of handling at the lab. Relative identifications assigned to the pipe are as shown in Figure 3.

Figure 1 *– Photograph taken at the dig location showing the excavated length of pipe and the location of the rupture. At the time this photograph was taken, the rupture appeared to be coincident with the seam weld, but could not be conclusively determined due to the plastic wrap covering the ruptured length.*

Figure 2 *– Photograph of the rupture following removal of the plastic wrap covering. It was confirmed at this time that the rupture had a partial coincidence with the seam weld on the joint upstream of GW610, traversed GW610 and propagated in a clockwise direction in the base metal of the downstream joint. The red arrow indicates flow direction.*

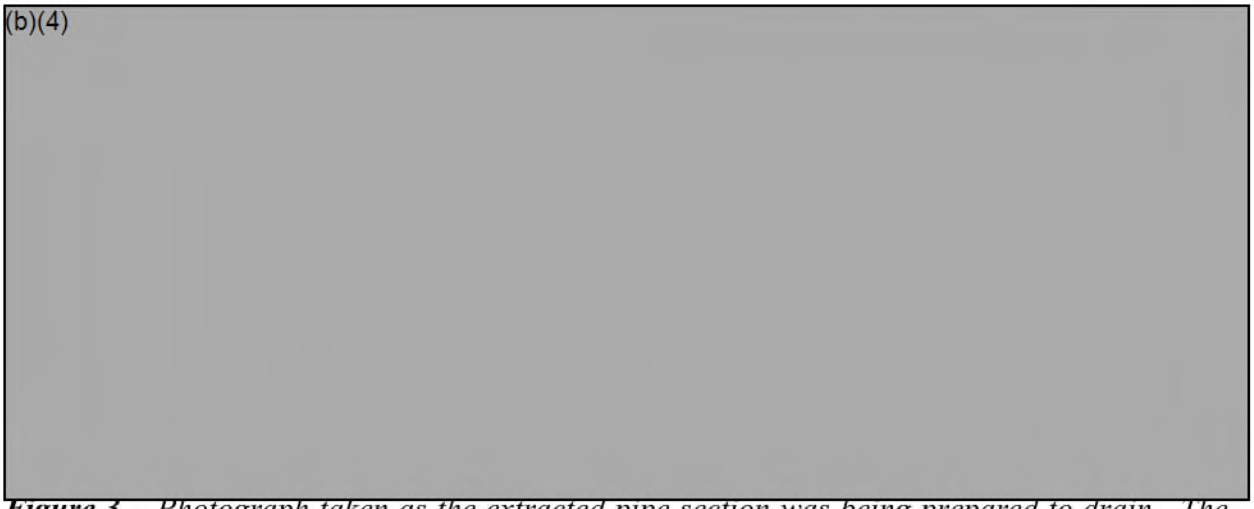

Figure 3 *– Photograph taken as the extracted pipe section was being prepared to drain. The yellow dashed line indicates the location of cutting. The section of pipe to the right of the dashed line was labeled "Pipe Section 1" and the section to the left was "Pipe Section 2", which contained the rupture.*

VISUAL EXAMINATION

General Condition

The visual examination of the pipe was conducted in the as-received condition. Both pipe sections were received with the fusion bonded epoxy coating (FBE) removed from the seam weld surfaces, and the unprotected pipe had visibly oxidized. This operation had been performed prior to transport for the purpose of performing non-destructive examination (NDE) on the seam weld prior to shipment. NDE examination was performed by Audubon.

The pipe sections appeared in fair condition overall and were observed to be free of any evidence of mechanical damage outside of the rupture region. There was no evidence of damage to the FBE coating remote from the rupture (blisters, dents, dings, gouges, scratches, etc.). The FBE coating in the immediate vicinity of the rupture was intermittently cracked and spalled off, however no evidence of a corrosive attack was observed on the exposed OD surfaces, indicating that the rupture event was responsible for the breaking of the FBE coating in the immediate vicinity of the fracture. The thickness of the coating as established via metallographic sectioning appeared uniform in the area of the rupture between (b)(4) mm and (b)(4) mm.

The general dimensions of the pipe sections were acquired and included diametric measurements in 6ft increments along the length of each joint (as able) and wall thickness measurements on each end. The diameter was measured using a pi-tape, the wall thickness was measured using pointed-tip micrometers. The diametric measurements are provided in Table 1, the measured wall thickness on each end are provided in Figures 6 and 7. Wall thickness measurements were acquired using pointed-tip micrometers along both sides of the fracture, in inch increments. Wall thickness measurements on the "seam weld-side" were taken in the base metal on the opposite side of the seam weld.

The Audubon axial measurements terminated around the rupture at (b)(4) (upstream side) and (b)(4) (downstream side). The rupture was partially coincident with and parallel to the seam weld. The widest displacement was measured at (b)(4) upstream of GW610. The widest measured displacement was (b)(4)

Figure 4 *– Overall photograph of Pipe Section 1 shown as received.*

(b)(4)

Figure 5 *– Overall photograph of Pipe Section 2 shown as received. The rupture was located in the central region of this pipe.*

Table 1 – Pipe Diameter

Pipe Identification	***Pipe Length [ft]***	***Linear Position [ft]***	***Pi-Tape Diameter [in]***
(b)(4)			

Figure 6 *– Wall thickness measurements on the ends of Pipe Section 1.*

Figure 7 *– Wall thickness measurements on the ends of Pipe Section 2.*

Table 2 – Base metal-side rupture wall thickness measurements

(b)(4)

Table 3 – Seam weld-side rupture wall thickness measurements

Distance from US End of Rupture [in]	***Wall Thickness [in]***	***Distance from US End of Rupture [in]***	***Wall Thickness [in]***
(b)(4)			

Features of Interest

Initial examination of the ruptured surface revealed a bow-shaped crack feature oriented consistent with an ID initiation event. It was further observed that this bow-shaped crack was coincident with the ID toe of the seam weld. There was initially no visually identifiable corrosion pitting associated with the feature observed during the visual examination.

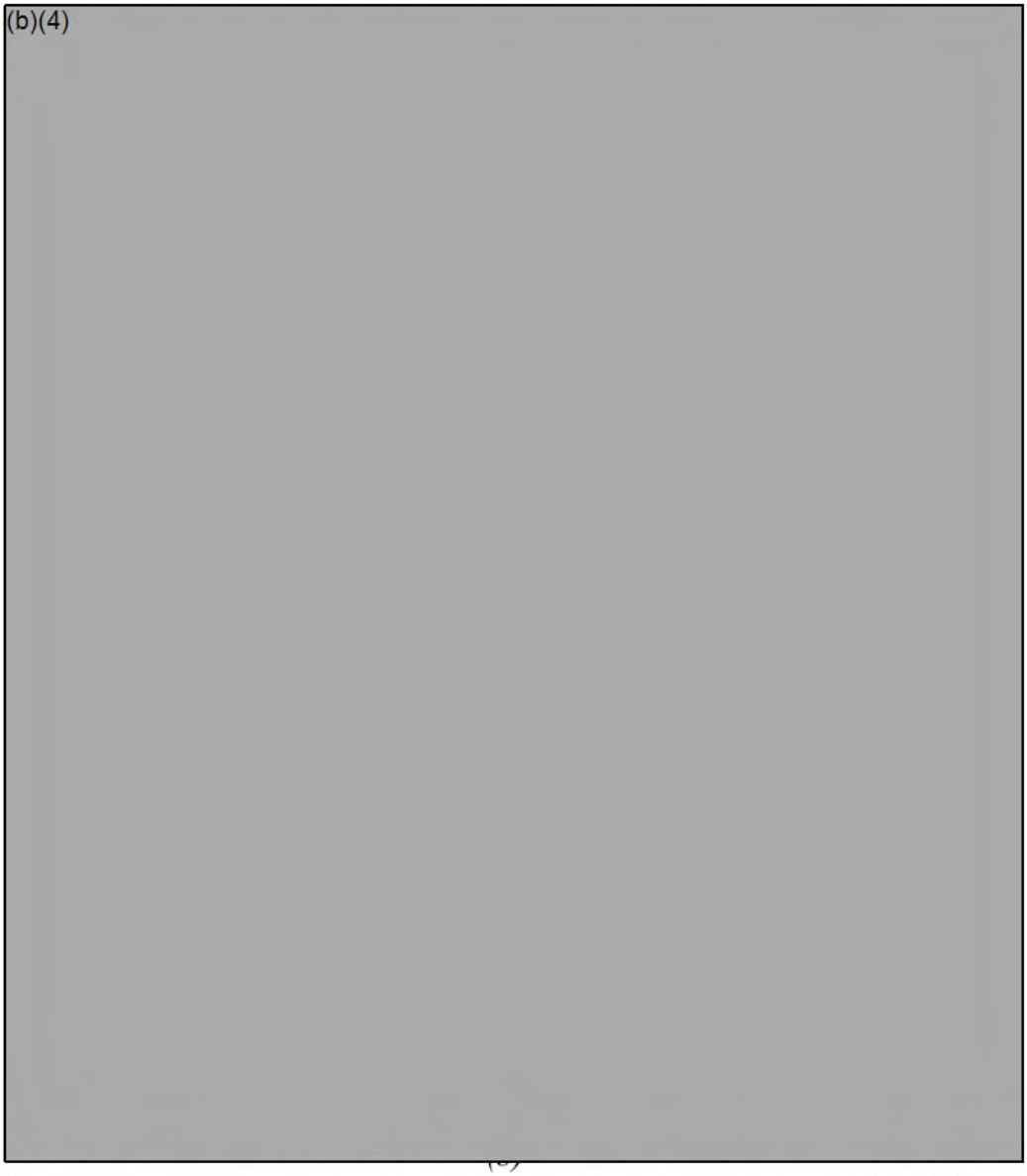

Figure 8 *– (a) The plastic wrap covering the rupture was intact upon receipt of the pipe. (b) Photograph showing the exposed rupture with the rubber hoses installed in Fort Ransom removed.*

Figure 9 *– Length and displacement measurements of the fish mouth rupture.*

Figure 10 *– Photograph showing initial documentation of the elliptical crack region on the base-side of the rupture.*

NON-DESTRUCTIVE TESTING

The seam weld of the failed joint and adjoining section of the downstream joint were grit blasted at the dig site following extraction to remove the fusion bonded epoxy (FBE) coating in preparation for non-destructive examination (NDE). The inspections were performed by Audubon and included diameter/ovality measurements, laser scanning, phased-array ultrasonic testing (PAUT), magnetic particle inspection (MPI), and peaking/out-of-round gaging. The individual reports are provided as Appendix D. None of the reported inspections identified any indications.

Following receipt and initial documentation of the pipes at Anderson & Associates, additional NDE inspections were undertaken to evaluate the girth weld (GW610) and the ligaments of the seam weld nearer the crack tips on either side of the rupture. The fracture was masked-off, and the sections to be evaluated were grit blasted to remove the FBE coating. The cleaned surfaces were then subsequently examined non-destructively by Audubon, who performed MPI, ultrasonic wall thickness measurements, and PAUT. No indications were noted in either the girth weld or remaining ligaments of seam weld near the upstream terminus of the rupture.

Figure 11 *– Photograph showing the rupture after grit blasting and secondary NDE examination. The panel encompassing the rupture to be removed is marked.*

The ID surface of the seam weld along the rupture was initially evaluated for indications using liquid penetrant testing (LP). This examination was performed after removal of the panel containing the rupture, and was done for the purpose of identifying any possible secondary cracks along the ID toes of the seam weld. A prerequisite to conducting this examination was to lightly degrease the ID surface to remove residual hydrocarbon sludge as residual surface debris can yield false-positive indications. Minimal cleaning was performed at this stage to avoid contaminating the fracture surface. As shown in Figure 12a, the results of the penetrant testing did not show any indications.

Subsequent to removal of the primary feature of interest, the seam weld in the ruptured area was re-examined non-destructively using white contrast magnetic particle inspection (WC-MPI), which is more sensitive with respect to LP. As shown in Figure 12b, there was an indication identified on the opposing toe of the seam weld to the fracture approximately 22 inches upstream of GW610. Metallographic documentation of this section is provided in Figures 48 – 53.

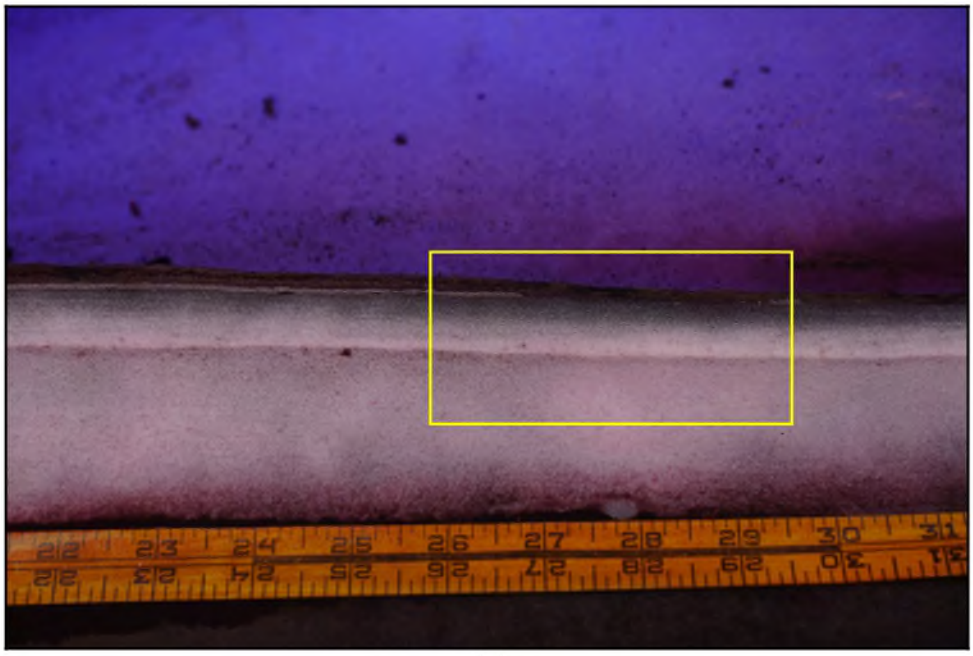

(a)

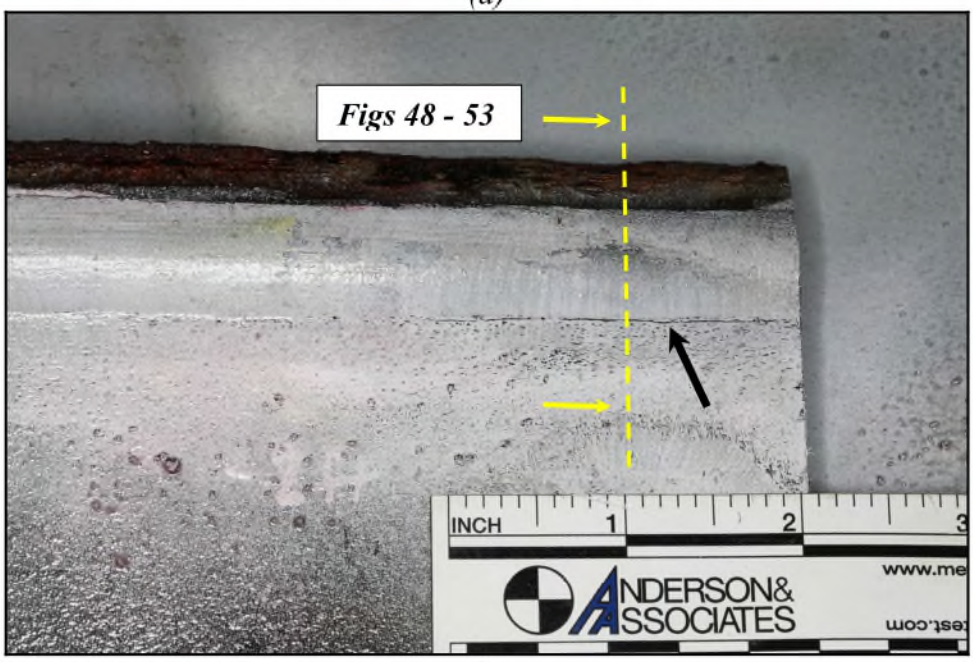

(b)

Figure 12 *– Photographs showing non-destructive test results on the ID seam weld in the ruptured panel using (a) liquid penetrant testing and (b) contrast magnetic particle inspection. No indication was identified with liquid penetrant, but an indication was noted on the toe opposite the rupture after wire brushing.*

FRACTOGRAPHIC EXAMINATION

Initial Examination

The fracture surfaces were initially examined prior to extracting the fish mouth from the pipe. The seam weld side of the fracture was caked with residual oil and soil, but the base side of the fracture was relatively clean. It was observed that there was an ID initiated, bow-shaped flat feature in the central region of the ruptured length coincident with the toe of the seam weld that was visually characteristic of a progressive cracking mechanism, and most consistent with fatigue cracking. Observations indicating fatigue as the cracking mechanism included the identification of three distinct zones: multiple ratchet marks along ID surface indicating multiple crack initiation points (Zone I), the flat nature of the progressive region (Zone II), and shear overload region (Zone III). The Zone II region exhibited a "bow-shaped" appearance, with the maximum depth located approximately (b)(4) upstream of GW610. The maximum measured depth of the fatigue region was (b)(4) nominal wall thickness, (b)(4) measured wall thickness) and the total length of the fatigue crack was approximately (b)(4) The fracture outside of the fatigued region consisted of shear lips, characteristic of fast-running ductile fracture. The fast-running fracture in the upstream direction propagated parallel to the HAZ for approximately 2 ft before deflecting into the base metal. The measured crack depths of the fatigued region on the base-side of the fracture are provided in Table 2.

Visual and Stereoscopic Examination

The fracture surfaces were visually examined in detail following the removal of the panel from the pipe body. In order to facilitate the examination, oil residue and debris were removed from the seam weld side of the fracture using a combination of cotton swabs, a wooden dowel, and a degreaser (Simple Green®).

Following the light cleaning, the fracture surface was examined using a Keyence digital microscope and observed to exhibit multiple crack arrest lines, more prominently visible on the fatigued surface nearer the transition to the sudden shear overload region. It was further observed that the ID edge of the fatigue crack appeared relatively smooth, though a fine dispersion of micro-pits were observed under higher magnification as shown in Figure 14. Figure 15 details

secondary cracking identified in the Zone II region. There were (b)(4) (b)(4) The orientation of the secondary cracks was perpendicular to the advancement of the fatigue crack, and appeared visually consistent with hydrogen induced cracking (HIC).

Table 2- (b)(4)

(b)(4)

20.0	11.5	0.080

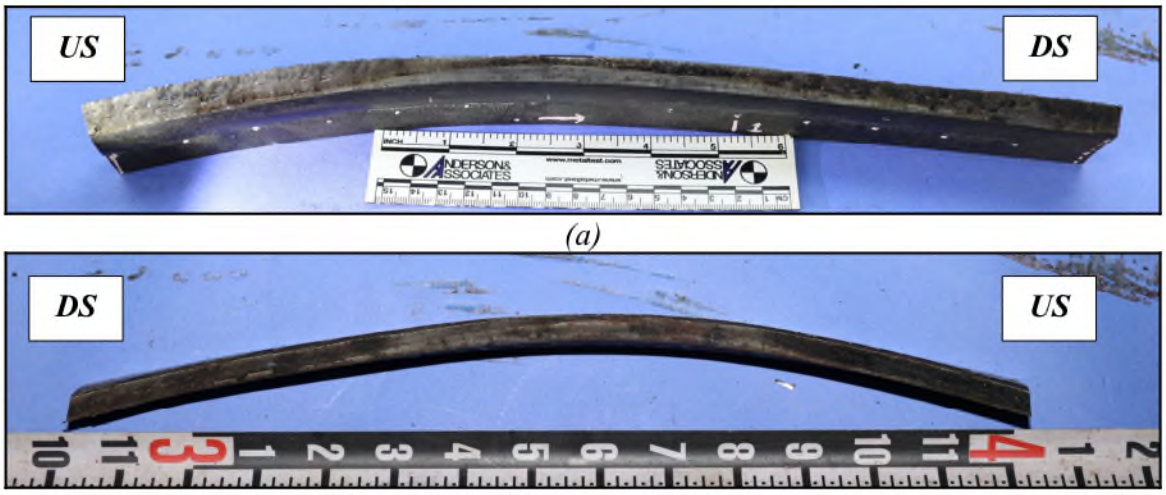

Figure 13 *– Overall view of the section of the seam-side crack surface encompassing the fatigue crack.*

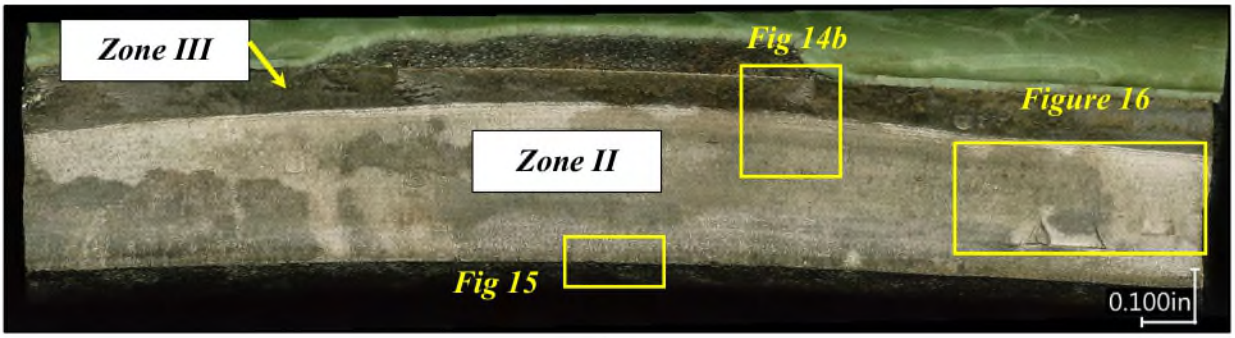

(a)

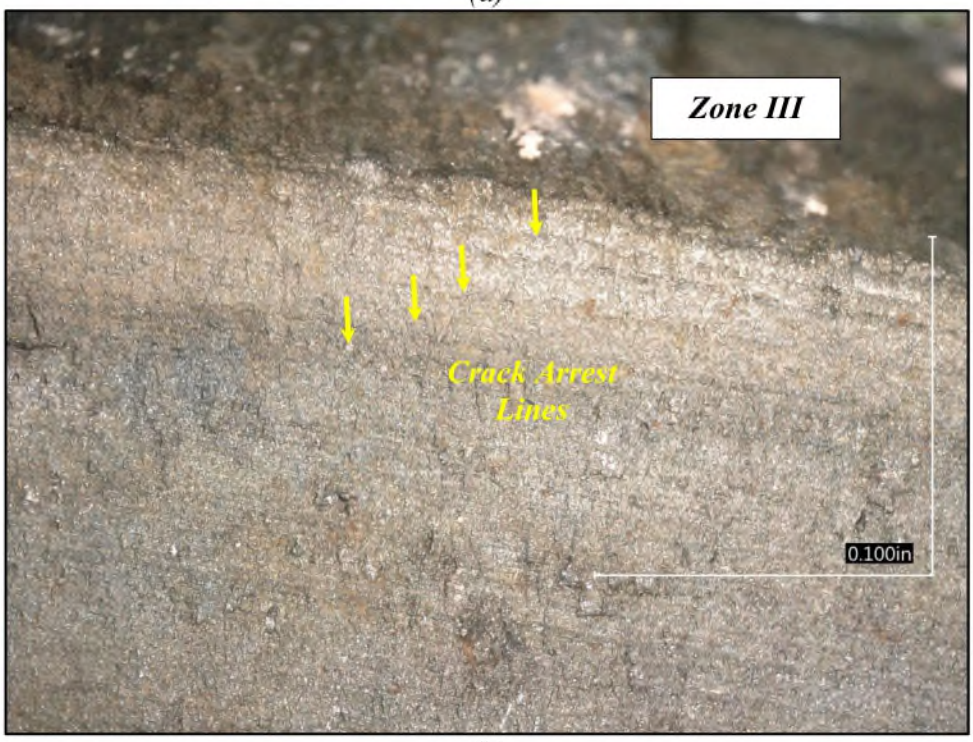

(b)

Figure 14 *– (a) Low magnification view detailing critical features observed on the cleaned fracture surface section encompassing the deepest fatigue region. (b)Higher magnification view showing multiple crack arrest lines on the fatigued surface near the ductile overload region (Zone III).*

(a)

(b)

Figure 15 *– (a) Oblique view of the seam-side of the fracture showing a fine dispersion of micropits on the ID surface adjacent to the weld toe. (b) Magnified view of the ID toe showing clusters of micropits.*

Figure 16 *– Low magnification view of several secondary crack-like features identified on the fatigued surface. The secondary cracks were oriented perpendicular to the fatigue crack growth direction. The secondary cracks appeared visually consistent with hydrogen induced cracking (HIC).*

SEM/EDS Examination

The sectioned portions of each elliptical crack features on the seam weld-side of the fracture were examined in the scanning electron microscope (SEM) using both backscatter electron contrast (BSE) and secondary electron imaging (SEI), the latter being more sensitive to surface topography. The seam weld-side was selected for the purpose of being able to evaluate the micro-pitting on the surface. Three sections of the fracture were examined, each encompassing varying degrees of progressive crack penetration and secondary cracking. Specimen 1 (SEM-1) was initially examined before cleaning so that the chemistry of the scale product on the surface could be examined using energy dispersive x-ray spectroscopy (EDS), the other two specimens were examined only in the cleaned condition. EDS is a qualitative chemical analysis technique that can accurately identify elements present on a surface but cannot identify compounds and only provides a semi-quantitative chemical composition. The results of the EDS analysis, shown

in Figure 17 showed (b)(4) (b)(4) Figure 18 shows a higher magnification view of a (b)(4) (b)(4)

(a)

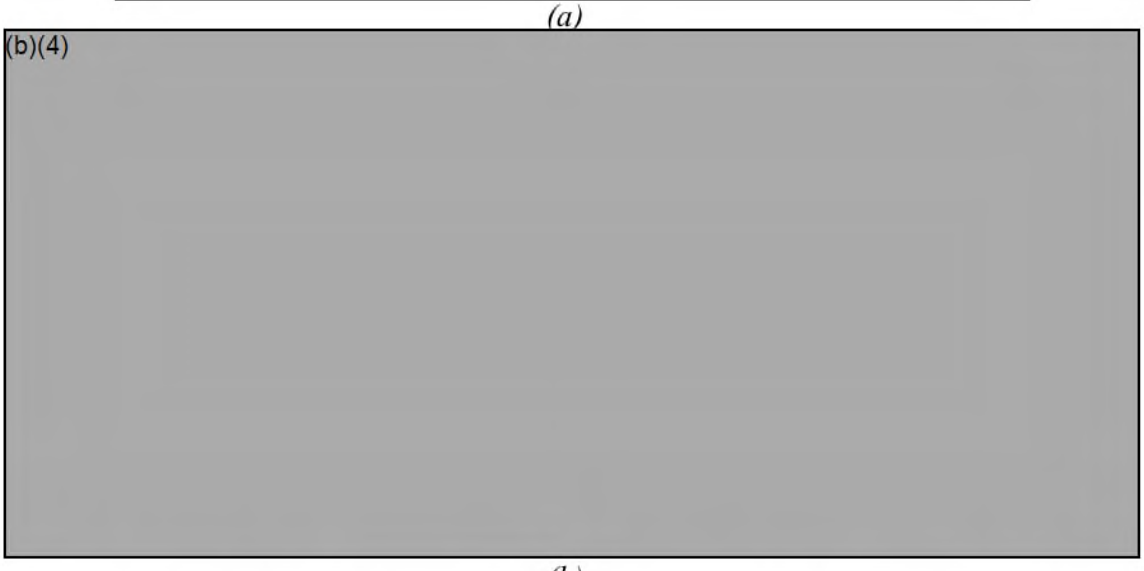

(b)

Figure 17 *– (a) Backscatter electron micrograph showing the fracture surface prior to cleaning. (b) The tabulated EDS data corresponding to this region shows elements typical of a crude oil and soil environment.*

(a)

(b)

Figure 18 *– (a) Backscatter electron micrograph showing a* (b)(4) *and (b) corresponding EDS results showing the* (b)(4) (b)(4) (b)(4)

Following the EDS examination of the surface of SEM-1, the section was cleaned using a combination of a dilute 2% Alconox solution and an ultrasonic bath. The purpose of the cleaning was to remove any residual hydrocarbon residue and debris that would obscure a direct observation of the fractured surface. Various regions of each sample were examined as shown in Figure 19, beginning with the crack initiation along the ID toe of the weld. As shown in Figure 20, radially oriented ratchet marks identifying multiple fatigue crack initiation points were observed. Some, but not all of the ratchet marks coincided with micro-pitting along the ID surface. Overall, the micro-pits exhibited hemispherical morphologies. The approximate depth the micro-pit shown in Figure 20b was less than 100µm in depth, or approximately the diameter of a human hair. Fractographic examination of the other two sections of the fracture exhibited identical fracture morphologies.

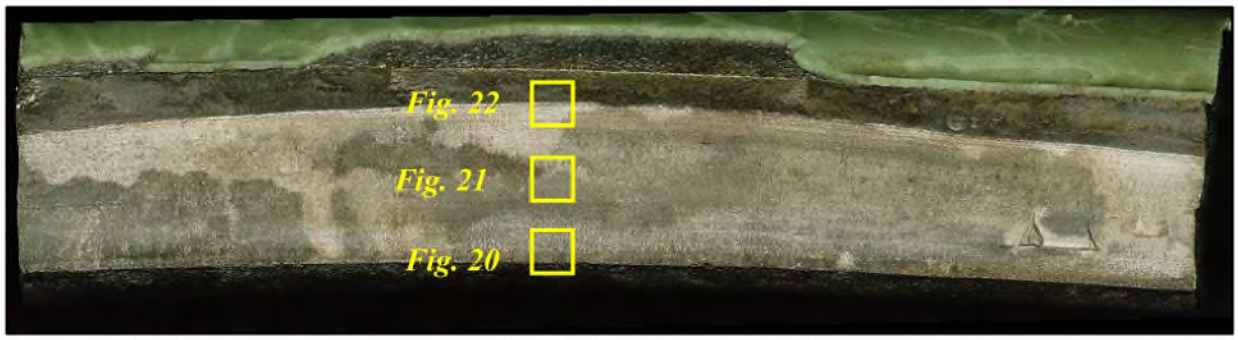

Figure 19 *– Low magnification view of SEM-1 post-cleaning showing the locations examined in the associated Figures.*

(a)

(b)

Figure 20 *– Backscatter electron contrast fractographs showing the coincidence of the fatigue crack with the ID toe of the weld. (a) Low magnification view showing* (b)(4) (b)(4) *(b) Higher magnification view showing a* (b)(4) (b)(4)

The morphology of the fatigue crack at mid-wall shown in Figure 21 was subsequently evaluated and numerous parallel crack arrest lines were evident. It appeared that the spacing of the parallel arrest lines increased as the crack propagated towards the OD, which is a feature consistent with increasing material compliance with increasing crack depth. It is important to note that these crack arrest lines visible at low magnifications would be inconsistent with striations, which are typically only observable at magnifications greater than 1,000X. At higher magnifications, the fracture surface exhibited a brittle cleavage morphology, with no evidence of striations observed.

(a)

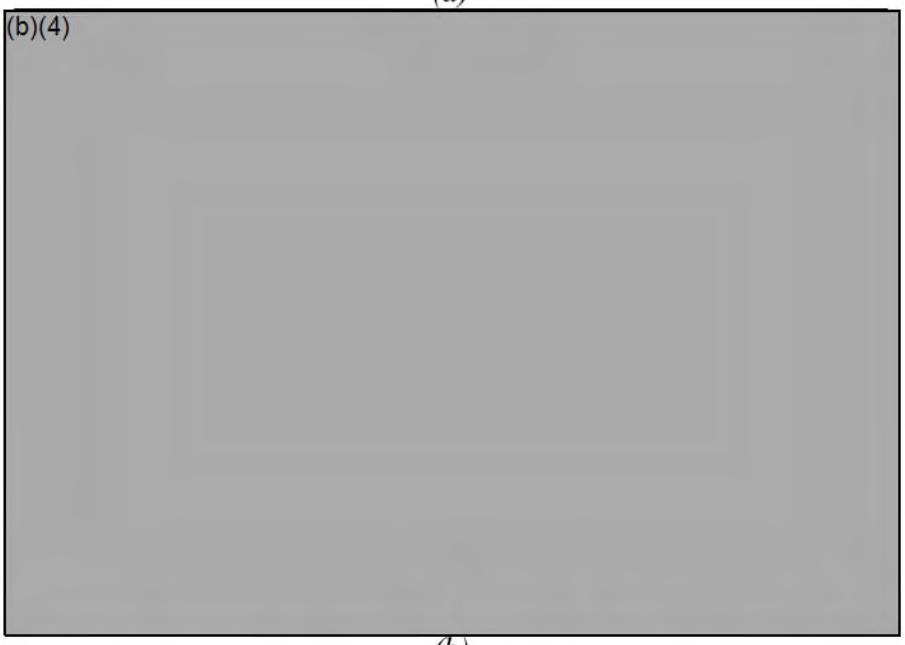

(b)

Figure 21 *– Secondary electron fractographs showing the fatigue crack morphology at mid-wall. At low magnifications as shown in (a), the fracture surface was characterized as having numerous crack arrest lines oriented perpendicularly to the crack growth direction. At high magnifications (b), the fracture surface exhibited features consistent with brittle cleavage.*

The morphology of the fatigue crack adjacent to the overload region shown in Figure 22 was examined and numerous parallel crack arrest lines were evident consistent with observations made at mid-wall. The spacing of the crack arrest lines appeared slightly larger near the transition zone. At higher magnifications, the fracture surface of this region again exhibited a brittle cleavage morphology, with no evidence of striations observed.

(a)

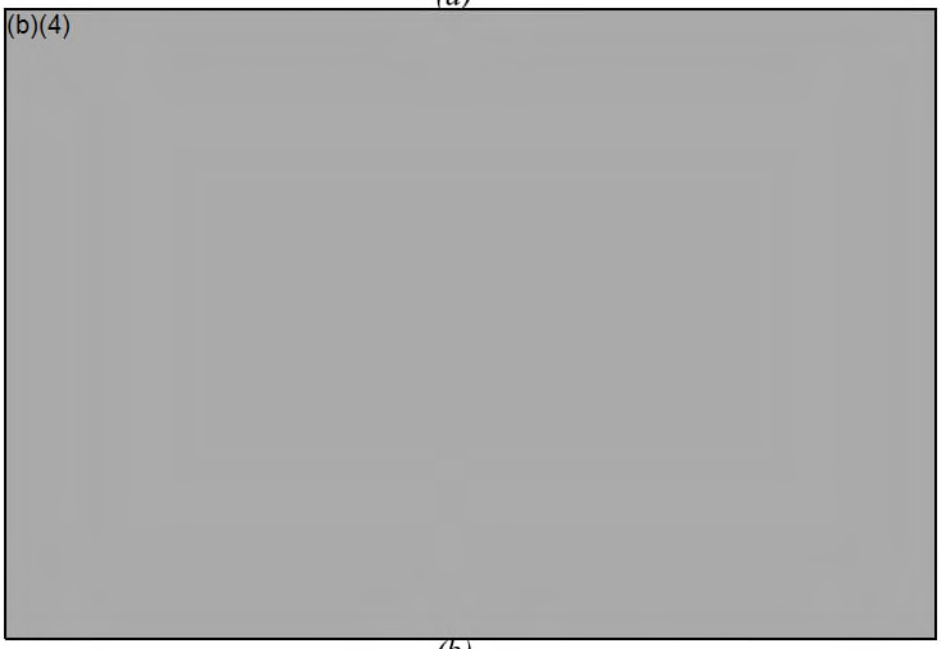

(b)

Figure 22 – (b)(4)
(b)(4)
(a) 30x (b) 1,000x.

A cursory fractographic examination of the Zone III region was performed and it was confirmed (b)(4) (b)(4) Representative fractographs are shown in Figure 23.

(a)

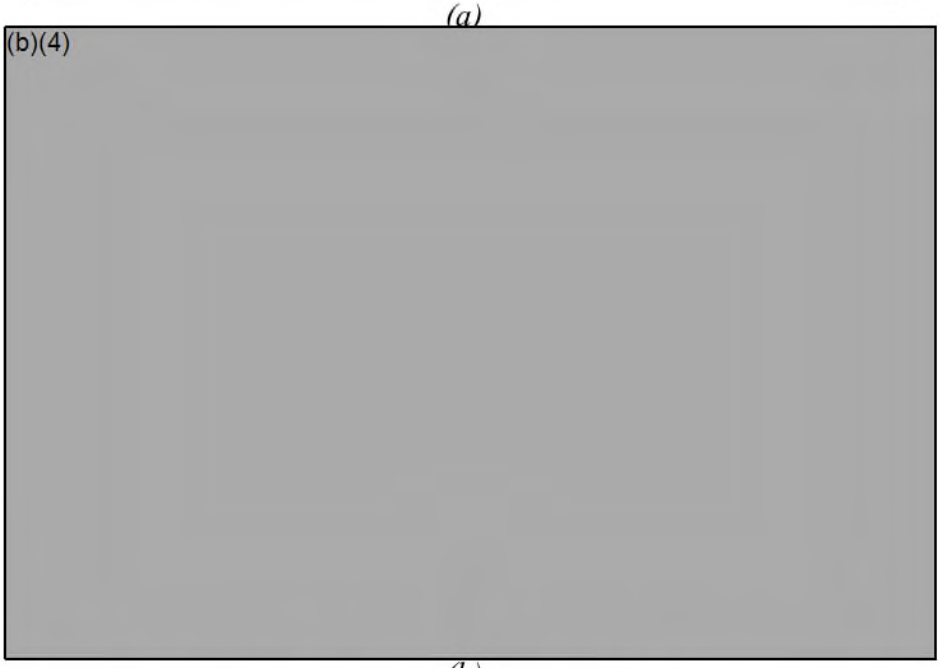

(b)

Figure 23 *– Secondary electron fractographs showing the* (b)(4) (b)(4) *(a) 30x (b) 250x.*

Examination of Secondary Cracks Identified on Fatigue Surface

Secondary cracks identified using low magnification were subsequently evaluated in the SEM. At low magnifications, each of these secondary cracks exhibited the following similar features:

- The advancing fatigue crack propagated around the secondary cracks.
- Each of the secondary cracks had ratchet marks on the "top" portion, further providing evidence that these features preceded the fatigue crack advancement.
- Evidence of lateral crack propagation with intergranular characteristics were evident.
- Several secondary cracks with visible exposed surfaces appeared smooth, in contrast with any ductile or brittle fracture mechanism.

Figure 24 *– Overall view of SEM-3 after cleaning highlighting a region* (b)(4)

(b)(4)

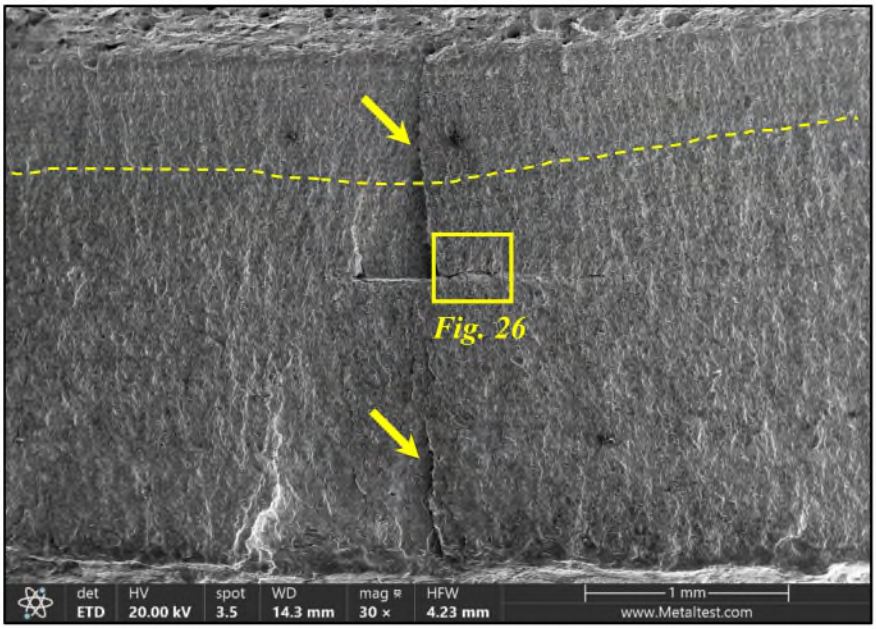

Figure 25 *– Low magnification secondary electron fractograph showing a perpendicular crack in the Zone II region. It was observed that the crack arrest lines propagated around the secondary crack, and ratchet marks were identified on both the ID surface and the "top" side of the feature as indicated with the yellow arrows. The arrows below and above the secondary crack identify ratchet marks, with the lower ratchet mark being coincident with the ID surface and upper ratchet being coincident with the secondary crack.*

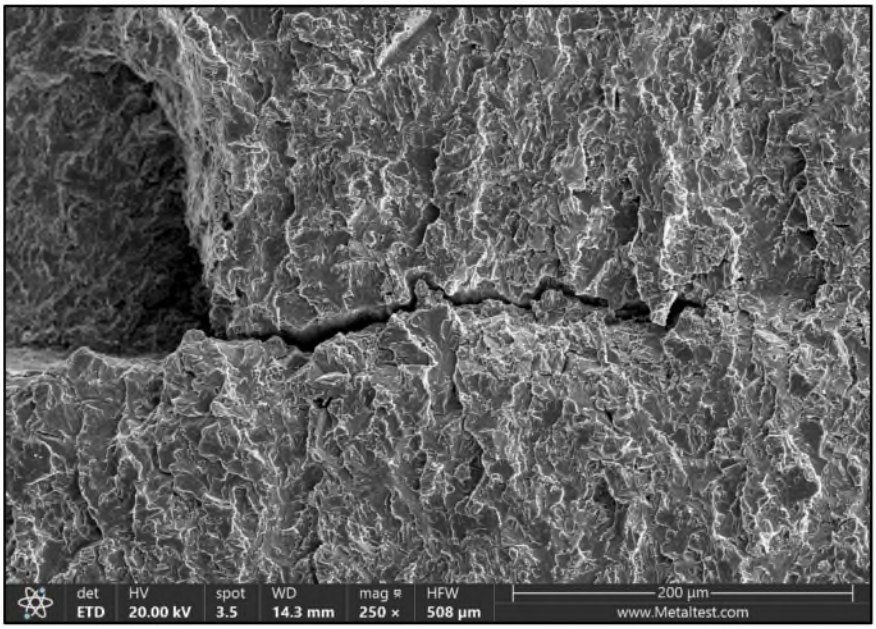

(a)

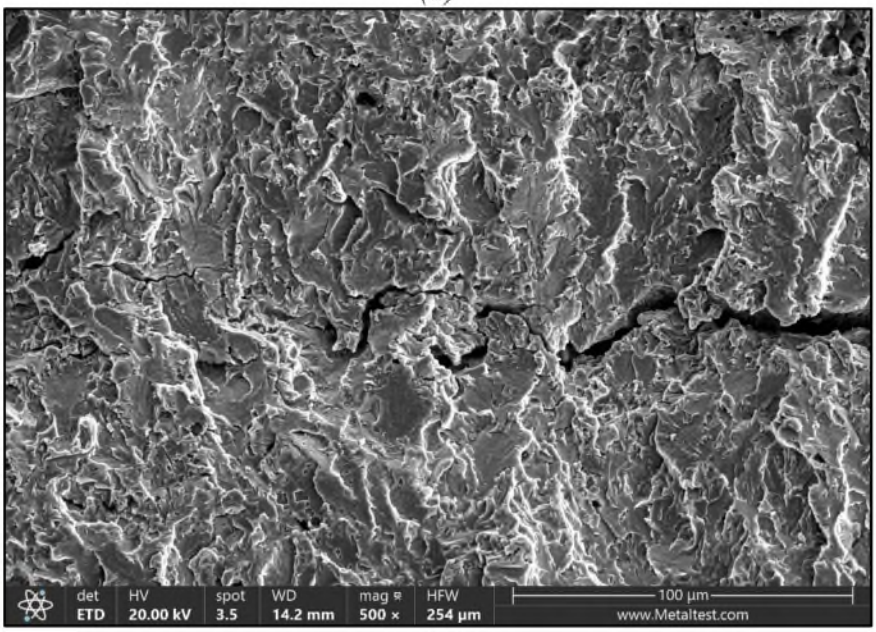

(b)

Figure 26 *– Secondary electron fractographs showing a perpendicular secondary crack located approximately at mid-wall. It was observed that there was crack extension, with intergranular characteristics propagating circumferentially from the central step.*

(a)

(b)

Figure 27 *– Secondary electron fractographs showing a separate instance of a perpendicular crack in the fatigue region. As was observed with other instances of this type of cracking, the crack arrest lines appeared to be influenced by the presence of the feature as evidenced by the bowing of the visible arrest lines on the OD side of the fracture. This instance appeared as a pocket in the material, and upon closer examination the exposed surface of the pocket appear smooth and devoid of evidence of a fracture event.*

Comparison of Tested Compact Tension Specimens to Fracture Surface

A fracture surface evaluation of tested compact tension (C(T)) specimens performed as part of the mechanical testing scope of this report for the purpose of comparing the fatigued portion of the tested specimen, to the fatigue surface on the rupture. Both HAZ and weld C(T) specimens were examined; the sample identifications were JH2-324-32-5 and JW3-324-32-10, respectively. As shown in Figure 28, it was observed that the fatigue pre-crack portion of each of the specimens exhibited a brittle morphology at low magnifications, and finely spaced striations at high magnifications.

The tested portion of the specimens was also examined and it was observed that HAZ specimens exhibited appreciably less ductile crack extension in comparison to the weld specimens. As shown in Figure 29, the HAZ C(T) specimen showed minimal ductile crack extension of approximately 250μm while the weld C(T) specimen exhibited significant ductile crack extension.

(a)

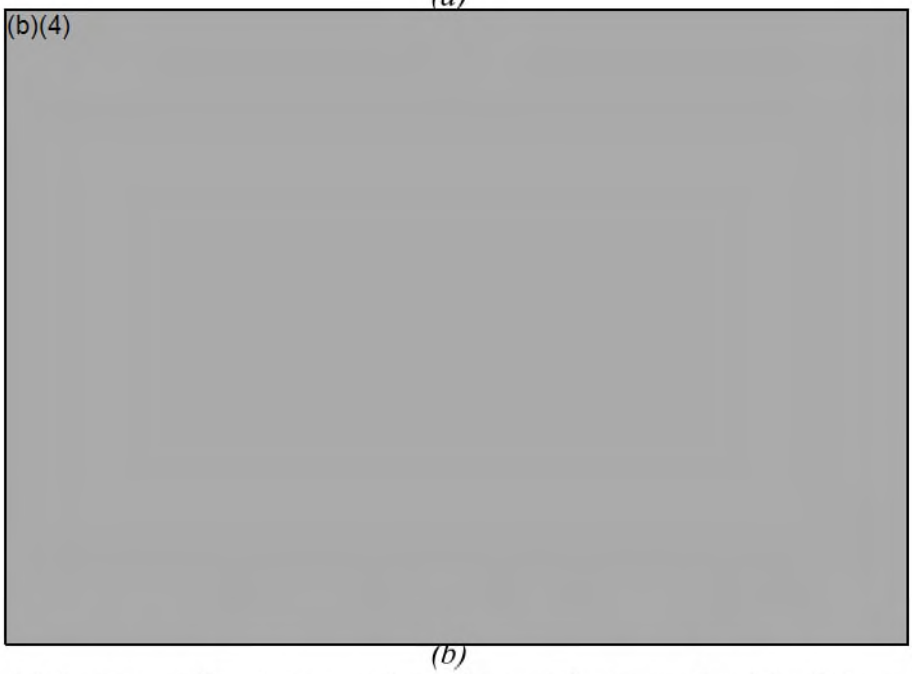

(b)

Figure 28 *– (a) Low magnification secondary electron fractograph of the fatigue pre-cracked surface of a HAZ C(T) bar from the failed joint. (b) High magnification secondary electron fractograph showing finely-spaced striations on the surface.*

(a)

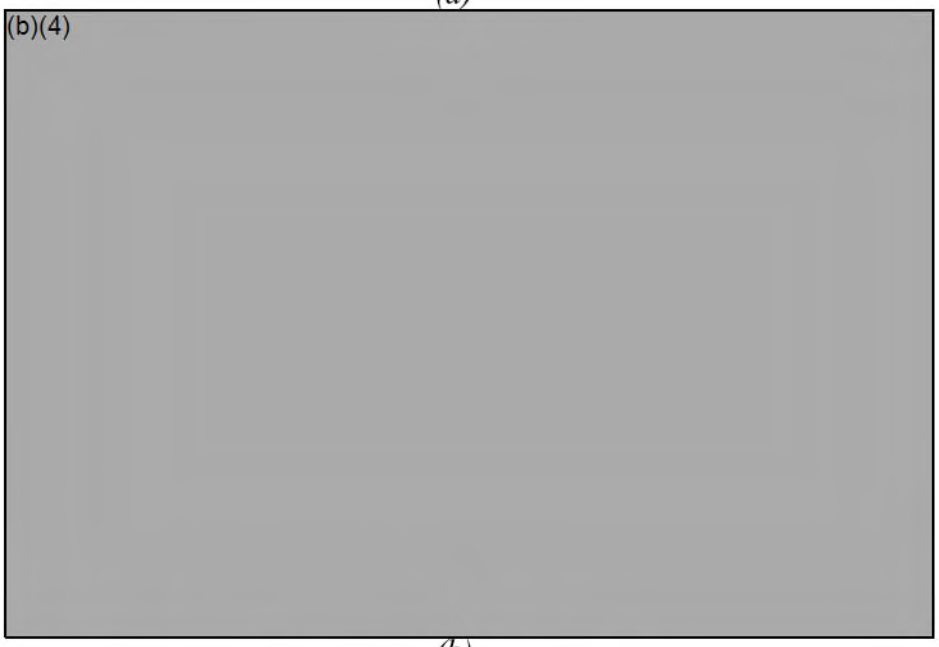

(b)

Figure 29 *– Secondary electron fractographs showing* (b)(4)

(b)(4)

METALLOGRAPHIC EXAMINATION

Transverse seam weld sections from the upstream, failed joint, and downstream joint were removed and metallographically prepared in accordance with ASTM E3. The samples were photodocumented in both the as polished and etched conditions; a 3% Nital solution was utilized to etch the microstructure. The focus of the examination of these specimens was to assess the overall weld quality and provide representative sections for geometric measurement.

It was assessed that the pipe was a double submerged arc weld (DSAW) construction, having been welded initially from the inner diameter (ID) and secondly from the outer diameter (OD). Each section was individually evaluated and each was found to be of good quality, showing no evidence of lack-of-fusion, cracking, porosity, or non-metallic inclusions. It was noted that there was significant (~3.8mm) weld misalignment between the centerlines of the ID and OD weld deposits on the failed joint, however there was complete fusion present.

The general microstructure of the weld deposits reflected an "as cast" structure, indicative that no subsequent thermal heat treatment was applied to the welds. The microstructure consisted of columnar ferrite, acicular ferrite, and pearlite (carbide). These microconstituents are typical of a low carbon steel weld deposit.

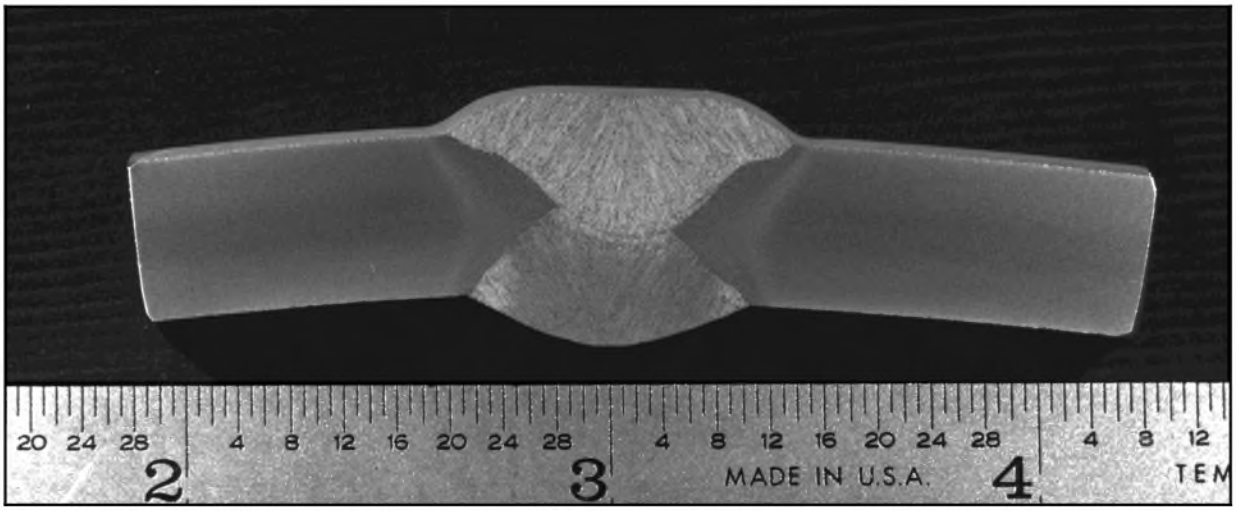

Figure 30 *– Metallographically prepared Upstream Joint macro section.*

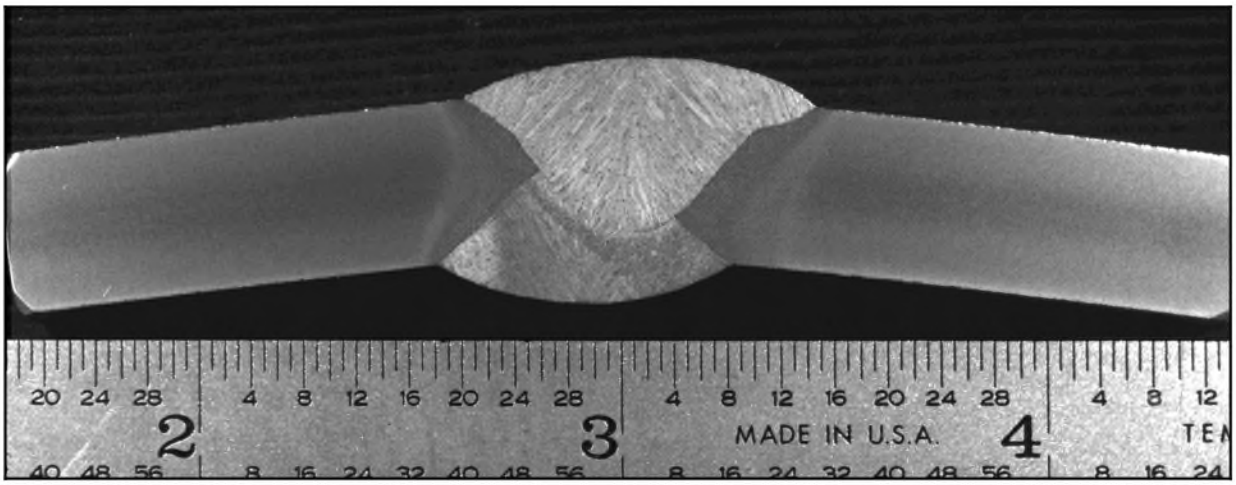

Figure 31 *– Metallographically prepared transverse seam weld macro removed from the failed joint upstream of the rupture.*

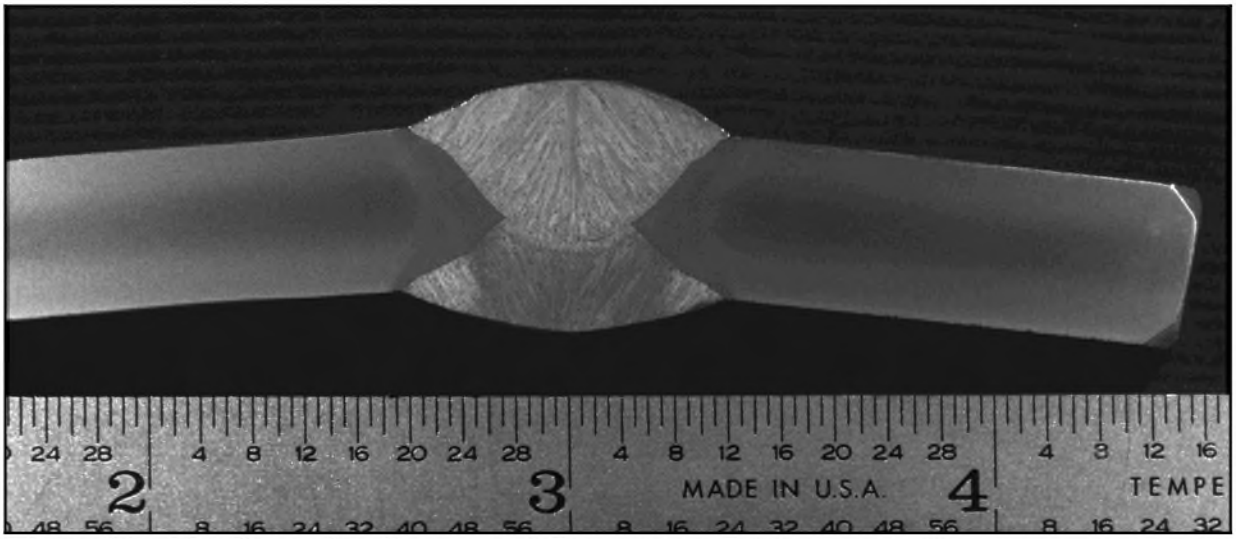

Figure 32 *– Metallographically prepared Downstream Joint macro section.*

Mated cross sections from the fatigued region of the crack were also metallographically prepared. Sections were cut from the region of deepest fatigue crack penetration (MET-1), ~50% fatigue crack wall penetration (MET-2), minimal fatigue crack wall penetration (MET-3), and one additional section encompassing a perpendicular crack in the fatigue section adjacent to the location where the minimal fatigue section was cut (MET-4). An overall view of the seam-side of the fracture showing the locations of each mated metallographic section is shown in Figure 33. Each metallographic section is addressed below.

Figure 33 *– Overall view of the seam-side panel containing the fatigue crack detailing the locations of the sections cut for metallographic examination.*

Deepest Fatigue Penetration

The location of the metallographic section and overall view of the prepared specimen are shown in Figure 34, the general observations were that the FBE coating on the OD surface appeared intact and tightly adhered with the exception of the area immediately surrounding the rupture location and that there was no evidence of general corrosion present on the ID surface. As shown in Figure 35, the crack propagated through the HAZ, and that no secondary or branched cracks were evident. Figure 36 details the crack initiation coincident with the weld toe, and that there were no defects or metallurgical anomalies present in the initiation location. Figure 37 shows the shear overload region at the OD surface, again demonstrating no metallurgical anomalies or defects were present, but a small secondary tear at the OD surface was present and likely associated with the plastic deformation of the pipe as it ruptured. Also evident at the OD surface was a lack of corrosion pitting or corrosion product accumulation.

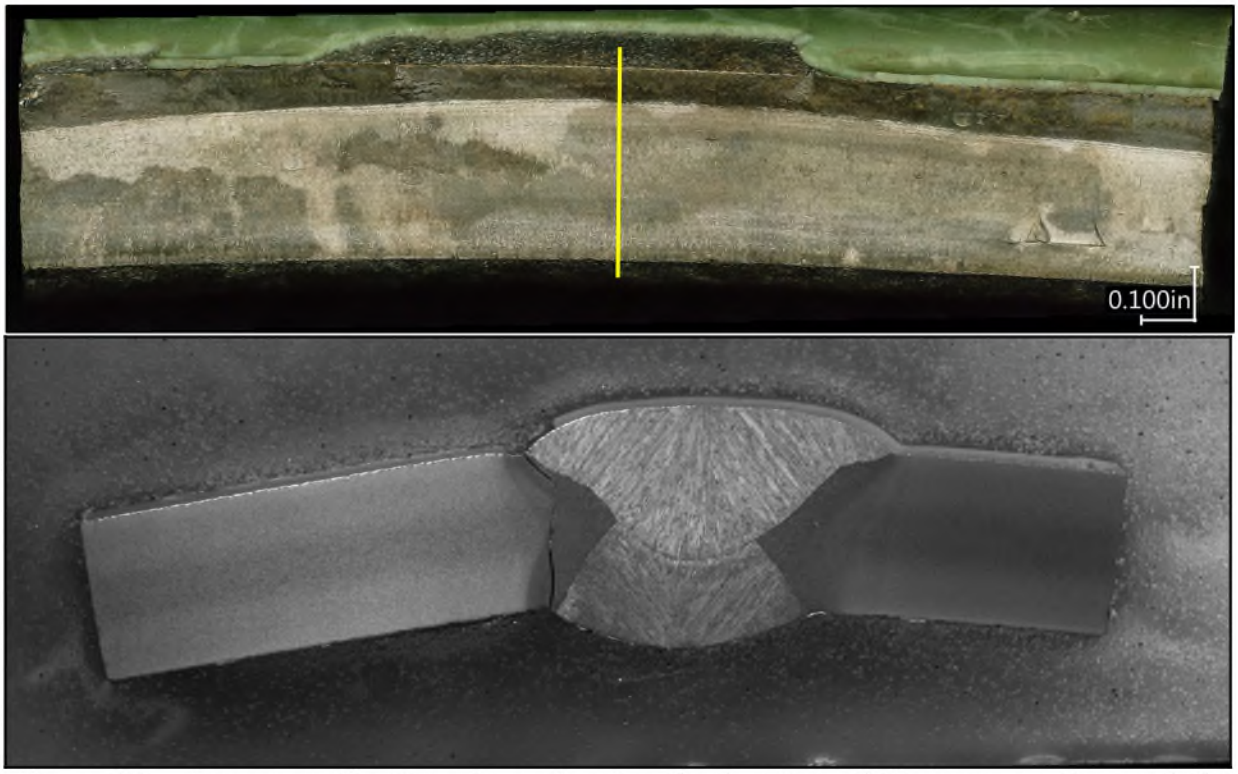

Figure 34 *– Low magnification views showing the location of the cross section and the metallographically prepared mated specimen.*

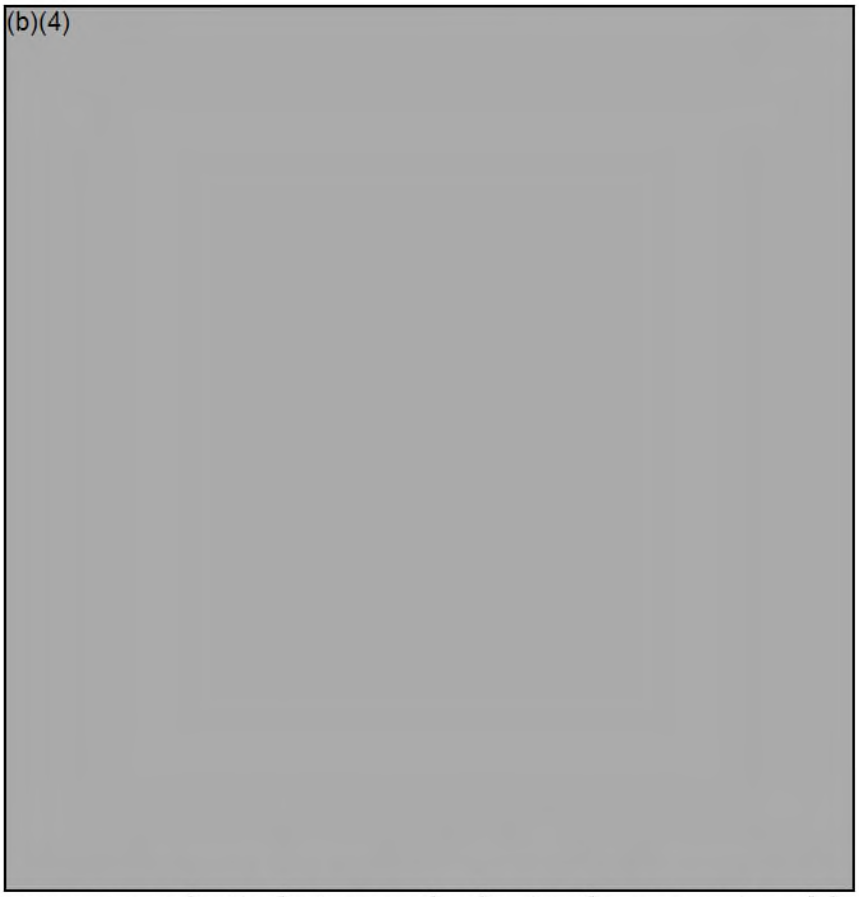

Figure 35 *– Photomontage of optical micrographs showing the progression of the fatigue crack through the HAZ from the toe of the weld. Originally photographed at 12.5x, 3% Nital etch.*

Figure 36 *– Optical micrograph showing the fatigue crack initiation coincident with the toe of the seam weld on the ID. 100x, 3% Nital etch.*

Figure 37 *– Optical micrograph showing the shear portion of the rupture on the OD surface. 50x, 3% Nital etch.*

50% Fatigue Metallographic Section

The section representing 50% fatigue crack penetration was specifically selected to intersect a secondary crack located within the Zone II region as shown in Figure 38. It was observed that there was no evidence of any inclusion present in this secondary crack, indicating it was unlikely to be associated with a non-metallic inclusion. It was further observed that the secondary crack was located in equiaxed, fine-grained microstructure, and that the crack was not associated with any microstructural feature.

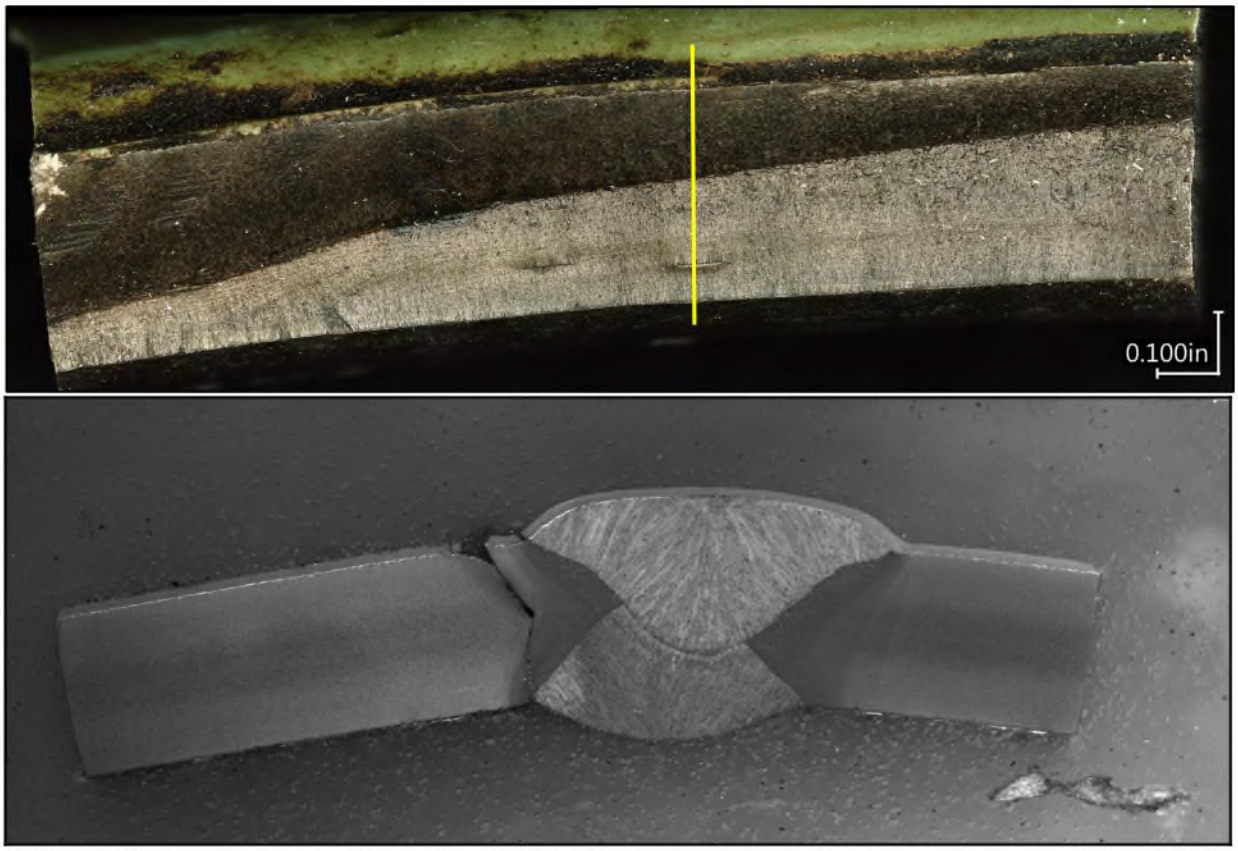

Figure 38 *– Location and metallographically prepared section through the region of 50% fatigue crack progression. This location was selected on the basis that it intersected a secondary crack on the fatigue surface.*

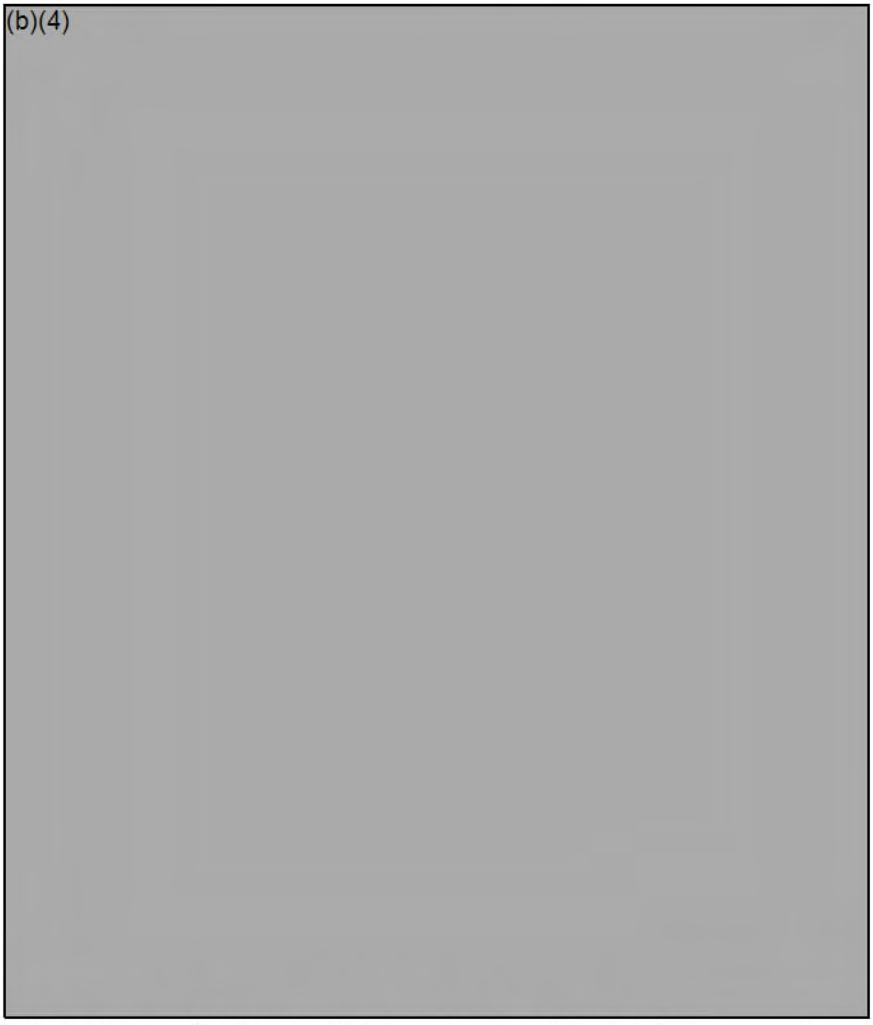

Figure 39 *– Photomontage of optical micrographs showing the* (b)(4) (b)(4) (b)(4) *Originally photographed at 12.5x, 3% Nital etch.*

Minimal Fatigue Metallographic Section

The metallographic section prepared through the location where only a small thumbnail of fatigue crack growth was observed is shown below in Figure 40. As with the previous metallographic sections, there were no metallurgical anomalies identified in the sample.

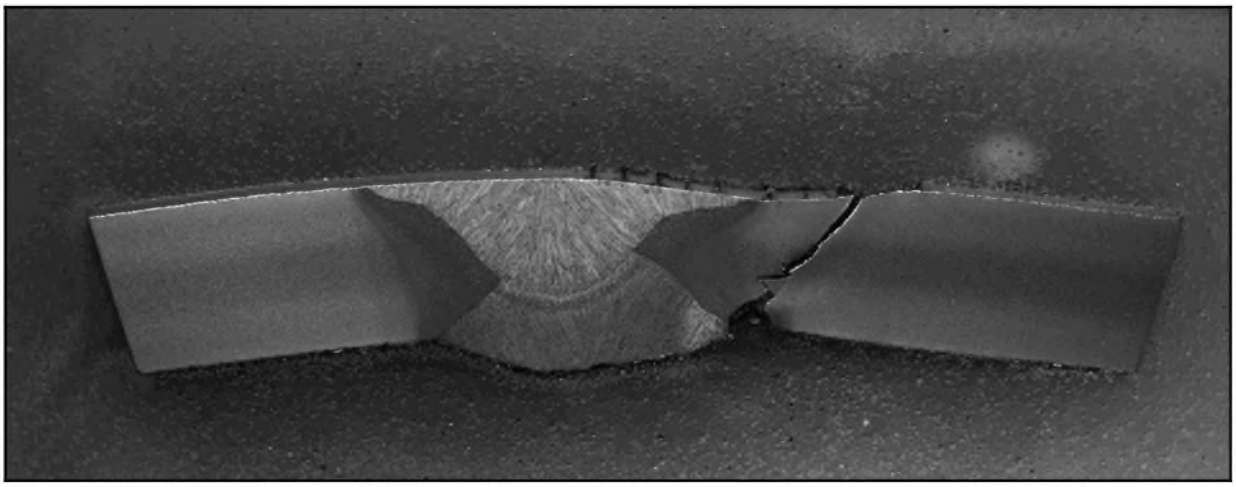

Figure 40 *– Overall view of the metallographically prepared section from the most downstream edge of the fatigue crack. Localized wall thickness reduction (necking) was evident, indicating the onset of ductile tearing.*

25% Fatigue Section Intersecting a Secondary Crack

The cut location and metallographically prepared section are shown overall in Figure 41. The pronounced nature of the secondary crack was evident in cross section, but not metallurgical or microstructural anomalies were identified to be associated with this feature as detailed in Figure 42. Coincidentally, this section intersected a small corrosion pit on the ID of the opposite toe of the weld, and upon closer inspection, a small crack was observed to be originating from the corrosion pit as detailed in Figure 43.

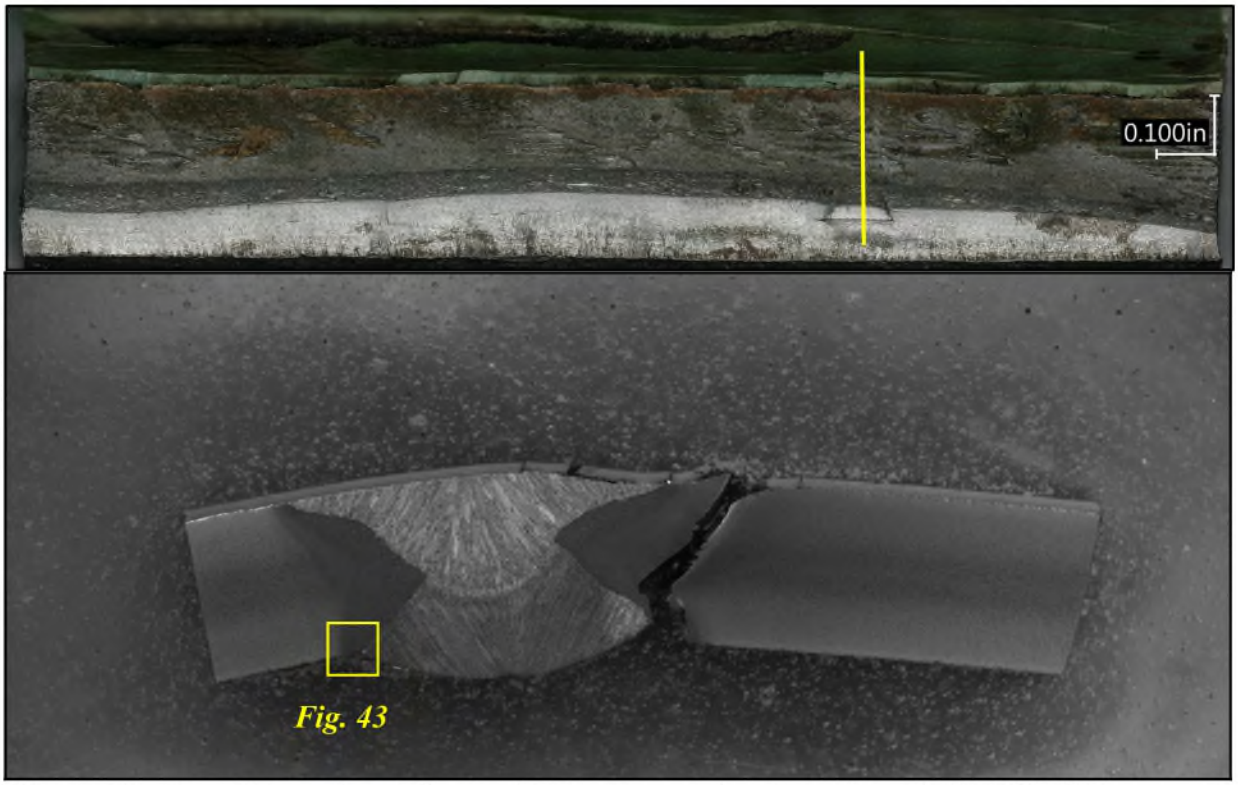

Figure 41 *– Location and metallographically prepared section through the 25% fatigue crack penetration location coincident with a large secondary crack.*

(a)

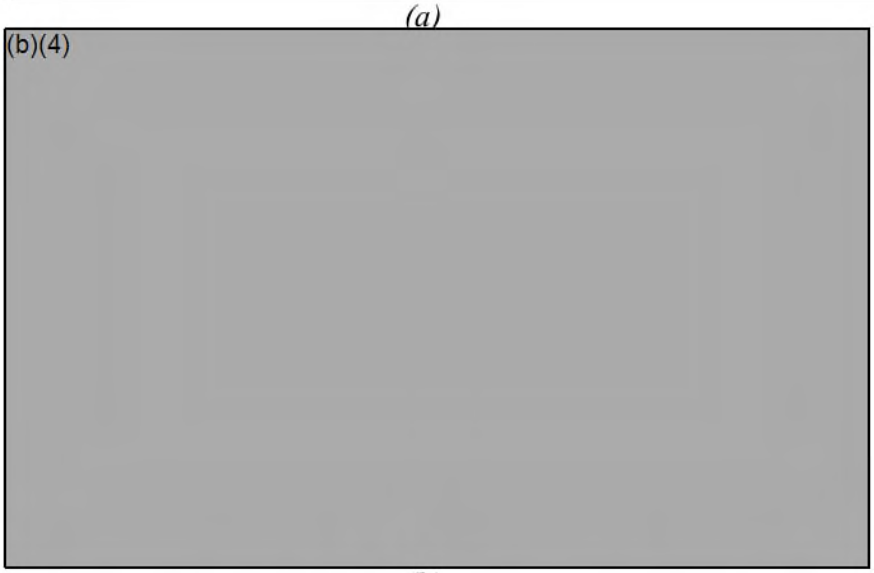

(b)

Figure 42 *– (a) Photomontage of optical micrographs showing the overall structure surrounding the rupture and secondary crack to be free of any metallurgical defects or anomalies, originally photographed at 12.5x. (b) Higher magnification optical micrograph showing the secondary crack to be transgranular and not associated with any metallurgical anomaly. Ductile tearing propagation parallel to the primary fracture is indicative that the flat secondary crack was present before the primary crack propagated through it. 100x, 3% Nital etch.*

(a)

(b)

Figure 43 *– Optical micrographs showing (a) low magnification view of the ID toe of the weld opposite the fracture and (b) high magnification view of a micro-pit with a crack originating from the pit.*

Metallographic Examination of the Pipe Base Metal

The microstructure of the base metal of the pipe was evaluated on longitudinally oriented cross section removed from GW610. The structure consisted of a fine-grained, essentially uniform structure of ferrite and pearlite that is typical of steel fabricated using a thermomechanically controlled process (TMCP). Representative micrographs showing the typical base metal microstructure of the failed joint are shown in Figure 44.

(a)

(b)

Figure 44 *– Optical micrographs showing the typical base metal structure at mid-wall consisting of fine-grained, banded ferrite and pearlite. The structure appeared typical for a TMCP steel product. (a) 100x (b) 500x, 3% Nital etch.*

Metallographic Examination of the Seam Weld HAZ

The heat affected zone (HAZ) associated with the seam weld was examined and found to show no metallurgical anomalies. The coarse-grained HAZ (CG-HAZ) had an acicular structure and the fine-grained HAZ (FG-HAZ) was more equiaxed. Both sides of the weld were examined and found to exhibit similar microstructural development as detailed below in Figure 45.

(a)

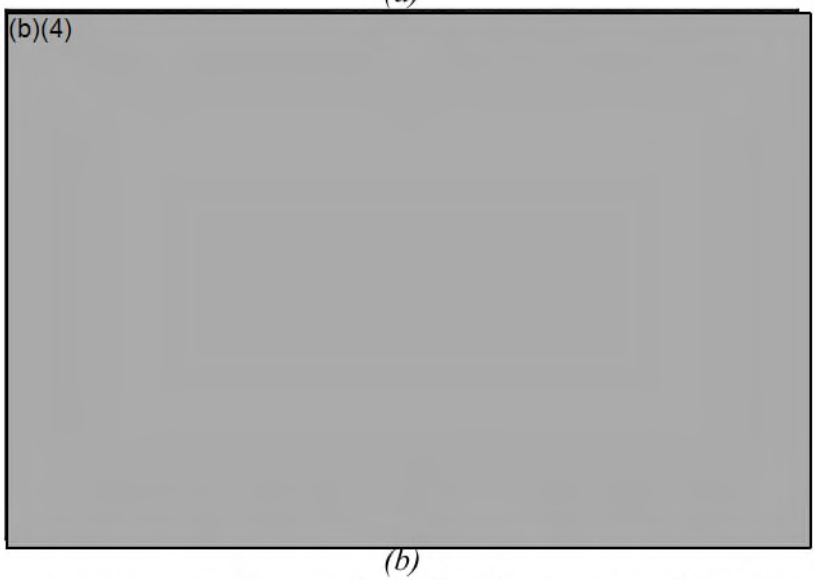

(b)

Figure 45 *– Optical micrographs showing the HAZ on both sides of the seam weld on the failed joint macro. (a) failed side (b) non-failed side. The microstructure on both sides appeared equivalent and consisted of both coarse and fine-grained regions. The coarse-grained region exhibited an acicular structure while the fine-grained region appeared more equiaxed. Both micrographs taken at 100x, 3% Nital etch.*

Metallographic Examination of Secondary Cracks Identified on the Fracture Surface

Characterization of the secondary cracks identified on the fracture surface was conducted to determine the most likely origin of the features, and to assess whether they may be associated with any feature or abnormality in the microstructure. As shown in Figure 46, the microstructure in the location of the secondary crack appeared homogenous, consisting primarily of equiaxed ferrite with dispersed pearlite/carbide. There was no evidence of any inclusion having been present in the void space on the left side extension of the crack into the HAZ/base metal. Higher magnification of the tip of the secondary crack, shown in Figure 47a showed a small, intergranular crack extension into the microstructure as well as some minor microstructural deformation. As shown in Figure 47b, the secondary crack was observed to propagate transgranularly, as evidenced by the calving of individual grains. These features are more consistent with a HIC-type crack as opposed to a microstructural feature such as an inclusion or lamination.

Figure 46 *– Optical micrograph showing* (b)(4) *Photographed at 100x, 3% Nital etch.*

(a)

(b)

***Figure 47** – Optical micrographs showing (a) "base-side tip of the secondary cracking showing a small intergranular propagation from the tip and minor plastic deformation and (b) view of mating secondary crack surface on the "HAZ-side" showing no evidence of any inclusions or microstructural anomalies. Both micrographs taken at 500x, 3% Nital etch.*

Metallographic Section Prepared from Fast Rupture Region

An additional section for metallographic examination was prepared from the fast running fracture region upstream of the fatigue crack (approximately 22" upstream of GW610). This section also intersected the ID indication identified via MPI shown in Figure 12. (b)(4)

(a)

(b)

Figure 48 *– (a)* (b)(4) (b)(4) *(b)* (b)(4) (b)(4) *12.5x, as polished.*

Figure 49 – (b)(4)
(b)(4) *Originally photographed at 100x, 3% Nital etch.*

(a)

(b)

Figure 50 *– Optical micrographs showing the* (b)(4) (b)(4) (b)(4) *(a) 500x, as polished, (b) 500x, 3% Nital etch.*

(a)

(b)

Figure 51 *– Optical micrographs showing* (b)(4) (b)(4) (b)(4) *. (a) 500x, as polished, (b) 500x, 3% Nital etch.*

(a)

(b)

Figure 52 *– Optical micrographs showing the* (b)(4) (b)(4) (b)(4)

(a) 500x, as polished, (b) 500x, 3% Nital etch.

(a)

(b)

Figure 53 *– Optical micrographs showing the* (b)(4)

(b)(4)

Girth Weld Microstructural Examination

Three, cross girth weld sections from GW610 were removed for metallographic examination were prepared at approximately 120° intervals. Each section was found to be metallurgically sound, having no inclusions, porosities, or lack-of-fusion defects. The girth welds were also a DSAW construction, welded first from the OD and second from the ID. There appeared to be a double weld pass present on the OD. Photographs showing the macro-etched sections are provided in Figures 54 – 56.

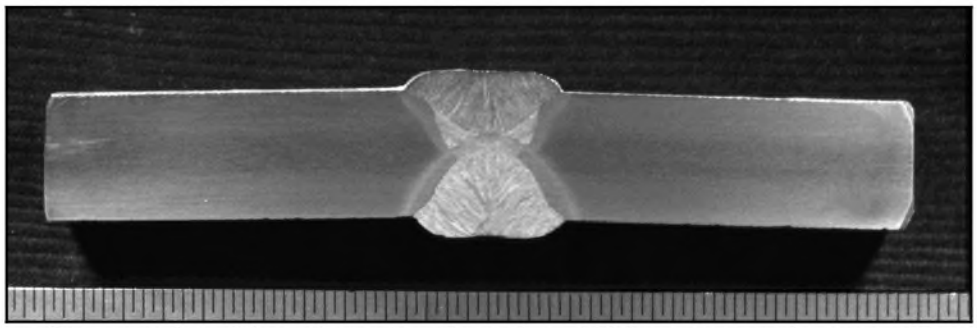

Figure 54 *– Cross girth weld section taken from the ~39° location on the pipe. The failed joint side is on the left.*

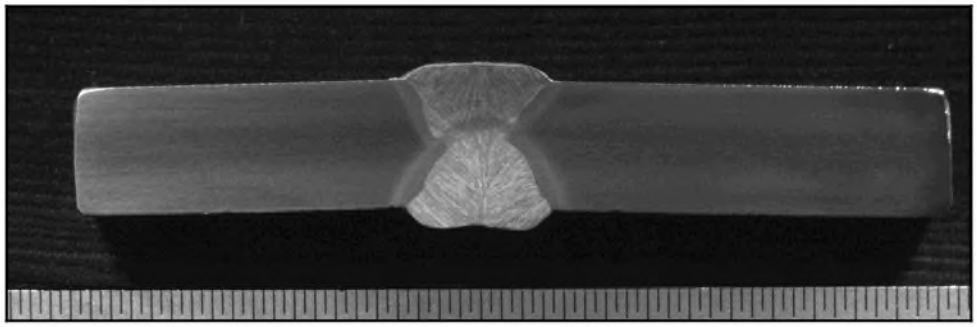

Figure 55 *– Cross girth weld section taken from the ~159° location on the pipe. The failed joint side is on the left.*

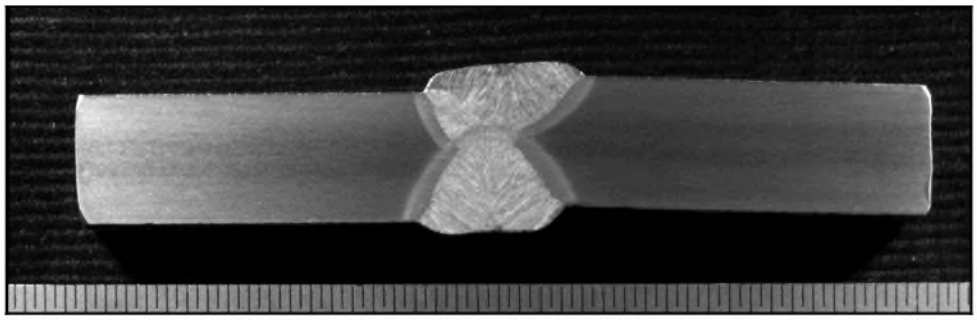

Figure 56 *– Cross girth weld section taken from the ~279° location on the pipe. The failed joint side is on the left. This section exhibited the most radial offset, measured at ~1mm.*

GEOMETRIC MEASUREMENTS

Geometric measurements were acquired on metallographically prepared specimens. The purpose was twofold: first to verify conformance of the weld geometry to the requirements of API 5L, 43rd Ed. and second, to measure the angles of the plate edges entering the weld (peaking/roof topping estimation), weld cap height, and radial offset, and weld out-of-line. The angular measurements were acquired using the peaking geometry described in Kopp et. al.[1]. The geometry of the weld, specifically radial offset and weld cap height were found to be within the specified limit of 1.6mm[2] and 3.2mm[3], respectively listed in the 43rd Ed.

There was misalignment between the ID and OD weld beads (out of line welds) noted on each of the failed joint metallographic sections; both the upstream and downstream joints exhibited no or minimal offset. The worst measured was ~3.76mm in the section removed remote from the rupture, and less severe in each of the mated cross sections from the rupture. The offset is acceptable per the 43rd Ed due to there being complete fusion between the beads. All measurements are shown in Figures 57 – 64. The angles shown in Figure 61a represent the angle between a plan perpendicular to the ID edge of the plates and the vertical centerline of the seam weld. The angles shown in Figure 61b be show the angle of the fatigue crack with respect to the perpendicular to the ID of the plate as well as the misfit angle of the mated surface.

[1] Gerhard Kopp, Michael Frank, Thomas Meinzer, and Roberto Yañez. "Improved Measurement of Peaking Angles and Peaking Height using ILI Data". Pipeline Technology Conference 2022, Berlin.
[2] API 5L, 43rd Ed., 7.8.2
[3] API 5L, 43rd Ed., 7.8.4

(a)

(b)

***Figure 57** – Measurements showing conformance of the upstream joint section with the maximum reinforcement cap height. (b) Angular measurements on the upstream joint metallographic section.*

(a)

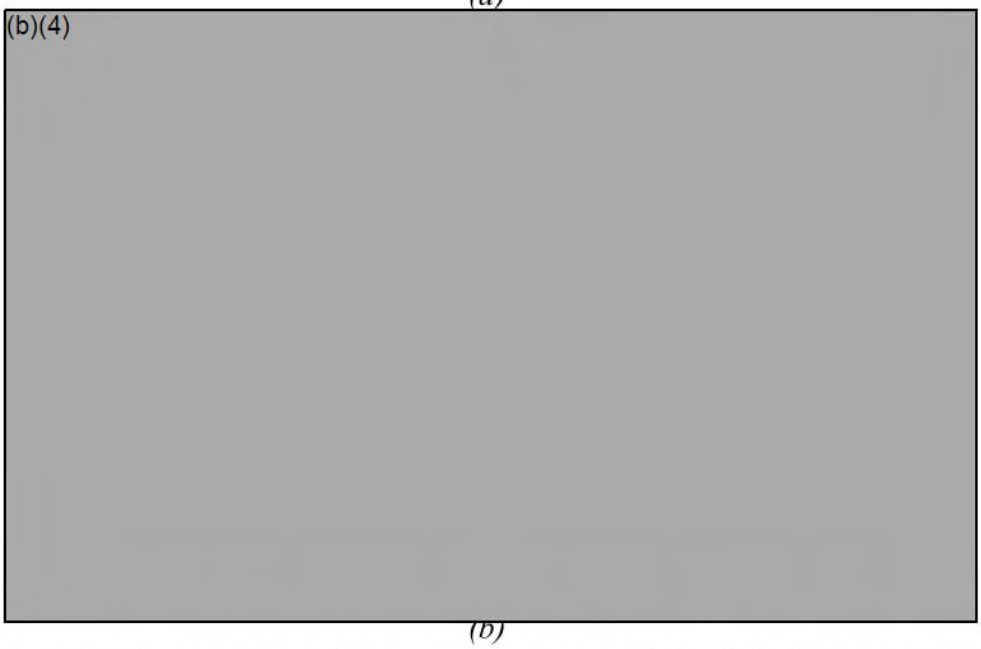

(b)

Figure 58 *– (a) Measurements showing conformance of the failed joint section with the maximum reinforcement cap height. (b) Angular measurements taken on the intact failed joint metallographic cross section.*

(a)

(b)

Figure 59 *– (a) Measurements showing conformance of the downstream joint section with the maximum reinforcement cap height. (b) Angular measurements on the downstream joint metallographic section.*

Figure 60 *– Cap height and radial offset measurements on the section with deepest fatigue crack penetration.*

(a)

(b)

Figure 61 *– (a) Angular measurements taken on the metallographic section through the deepest fatigue zone. (b) Angular measurements showing the mated misalignment of the mated section.*

(a)

(b)

Figure 62 *– (a) Cap height, radial offset, and out of line weld measurements on the section of 50% fatigue penetration. (b) Angular measurements on the 50% fatigue propagation specimen.*

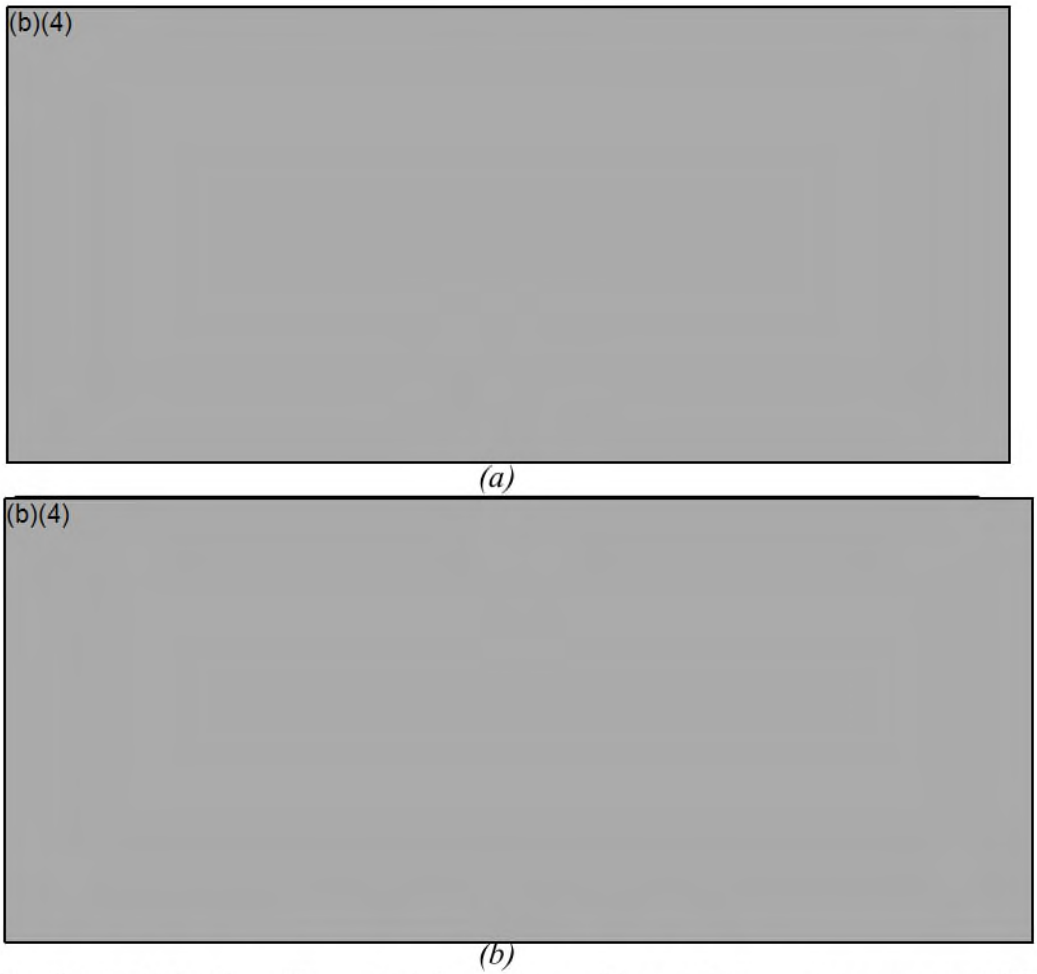

Figure 63 *– (a) Radial offset, ID cap height, and out of line weld measurements on MET-3 (b) Angular measurements on the mated section.*

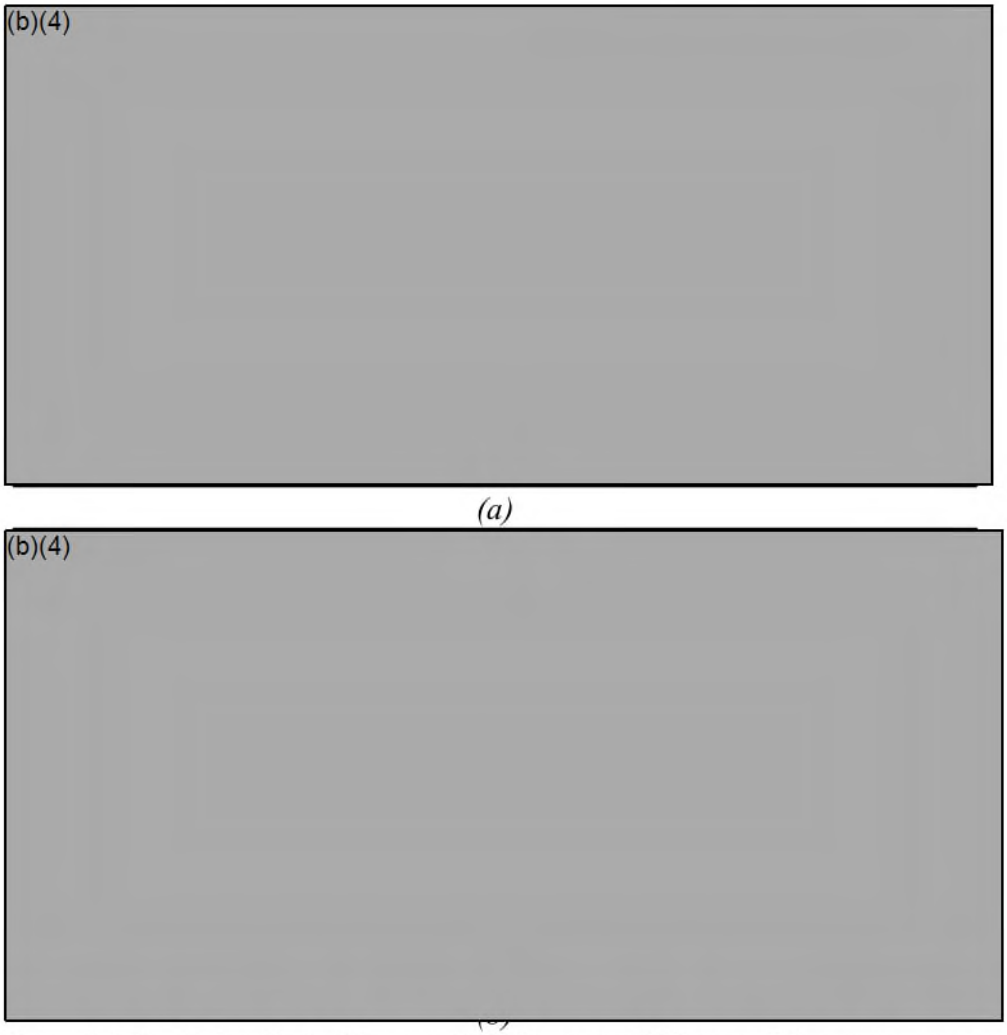

Figure 64 *– (a) Radial offset, ID cap height, out of line weld measurements on the metallographic section of the 25% fatigue zone. (b) Corresponding angular measurements.*

MECHANICAL TESTING[4]

Tensile Testing

Tensile testing of the pipe joints was conducted in accordance with API 5L 43rd Ed. and MPS-BSPC-TC-03 Rev. 1. Cross girth weld tensile testing was conducted in accordance with API 1104. Tensile testing consisted of both full wall thickness and sub-size round test specimens. The results of the tests are summarized in the following tables. The tensile datasheets for the full-wall thickness pipe specimens are included as Appendix E and the tensile datasheets for all sub-size tensile specimens are included as Appendix F.

Results of full-size, reduced section tensile testing (RST) are summarized below. (b)(4)

(b)(4)

Upstream Joint Full-Wall Thickness RSTs					
Specimen	Location Relative to SW [°]	0.5% EUL Yield Strength [Ksi]	Tensile Strength [Ksi]	Elongation in 2" [%]	Minimum Elongation[5] [%]
(b)(4)					

[4] Individual specimen identifications were established on the basis of clock position and axial length on the respective joint. For example, sample 324-33-9 indicates the specimen was removed from clock position 324°, and axial position on the joint was 33ft 9in.

[5] *minimum elongation* = $625{,}000(Acx^{0.2}/UTS^{0.9})$

Failed Joint Full-Wall Thickness RSTs

(b)(4)

Downstream Joint Full-Wall Thickness RSTs

(b)(4)

Upstream Joint Sub-Size 0.252" Cross-Weld Tensile Specimens

(b)(4)

[6] "TW" defined as transverse weld.

Failed Joint Sub-Size 0.252" Cross-Weld Tensile Specimens

(b)(4)

Downstream Joint Sub-Size 0.252" Cross-Weld Tensile Specimens

(b)(4)

Upstream Joint Sub-Size 0.252" Base Metal Tensile Specimens

(b)(4)

[7] "TB" defined as transverse base.

Failed Joint Sub-Size 0.252" Base Metal Tensile Specimens

(b)(4)

Downstream Joint Sub-Size 0.252" Base Metal Tensile Specimens

(b)(4)

CVN Impact Testing

Sets of 3/4-size[8], transverse oriented Charpy V-Notch (CVN) impact specimens were removed from each of the joints. Specimens were removed and notched in accordance with the guidance of API 5L, 43rd Ed. The specimens included base metal specimens removed 90° from the seam weld, seam weld HAZ (FL + 1mm), and seam weld centerline. The specimens were prepared and tested in accordance with ASTM A370 at -5°C[9]. Measured absorbed impact energies were converted to equivalent full-size results for comparison. The results demonstrate that the pipes met the minimum absorbed energy requirement of 30 ft-lb for API 5L grade X70 PSL 2 pipe, as well as the 33 ft-lb minimum specified in MPS-BSPC-TC-03 Rev. 1. Photographs showing the notch locations on the HAZ and weld specimens are included as Appendix G. The impact toughness values obtained during this testing when compared to the values listed in the respective MTRs were generally similar, though it should be noted that different sample sizes were utilized.

[8] API 5L 43rd Ed. specifies 2/3-size; MPS-BSPC-TC-03 Rev. 1 specifies largest obtainable sub-size specimen. 3/4 was the largest obtainable size.
[9] API 5L 43rd Ed. test temperature is 0°C, MPS-BSPC-TC-03 Rev. 1 specifies -5°C.

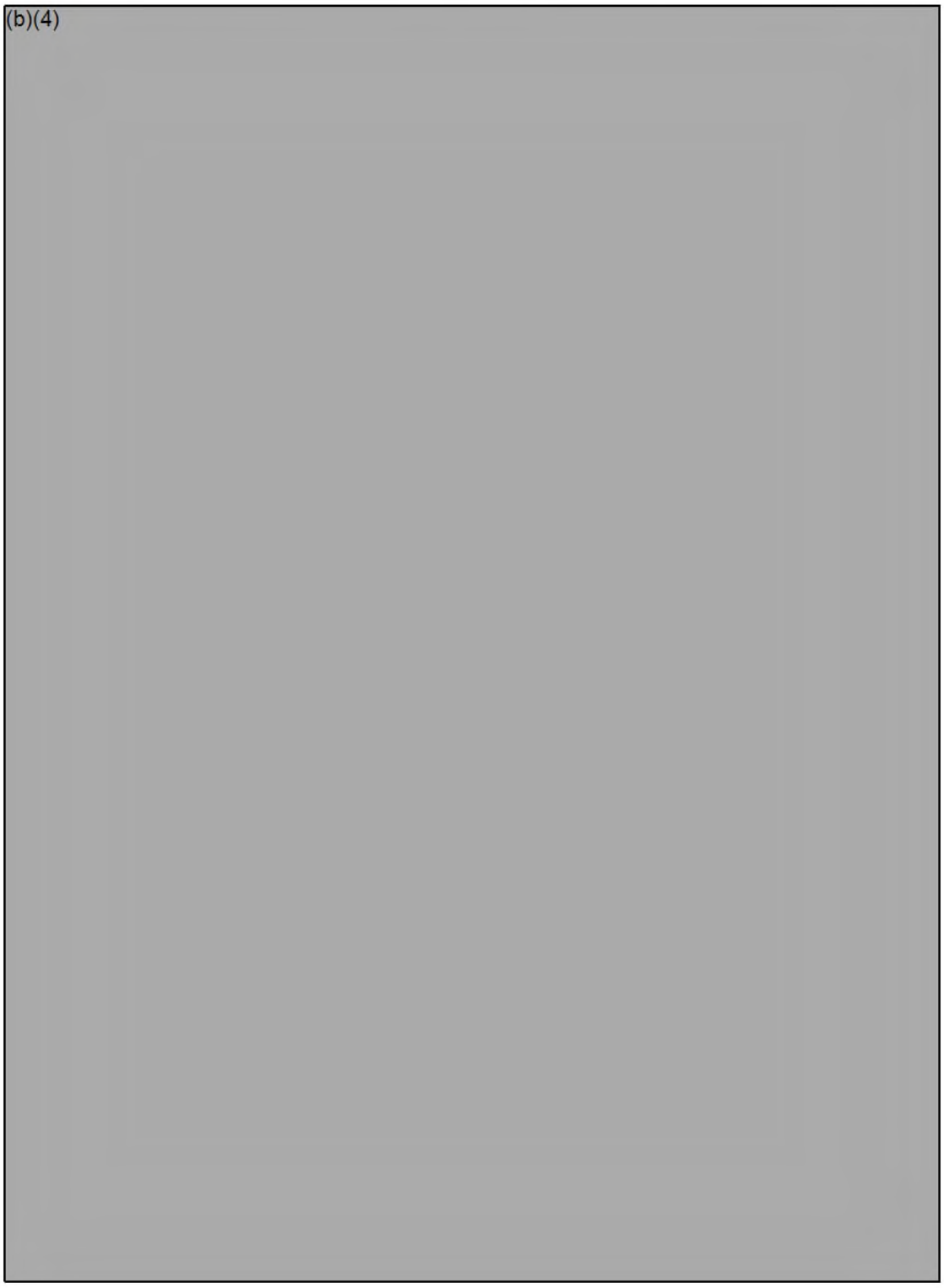
(b)(4)

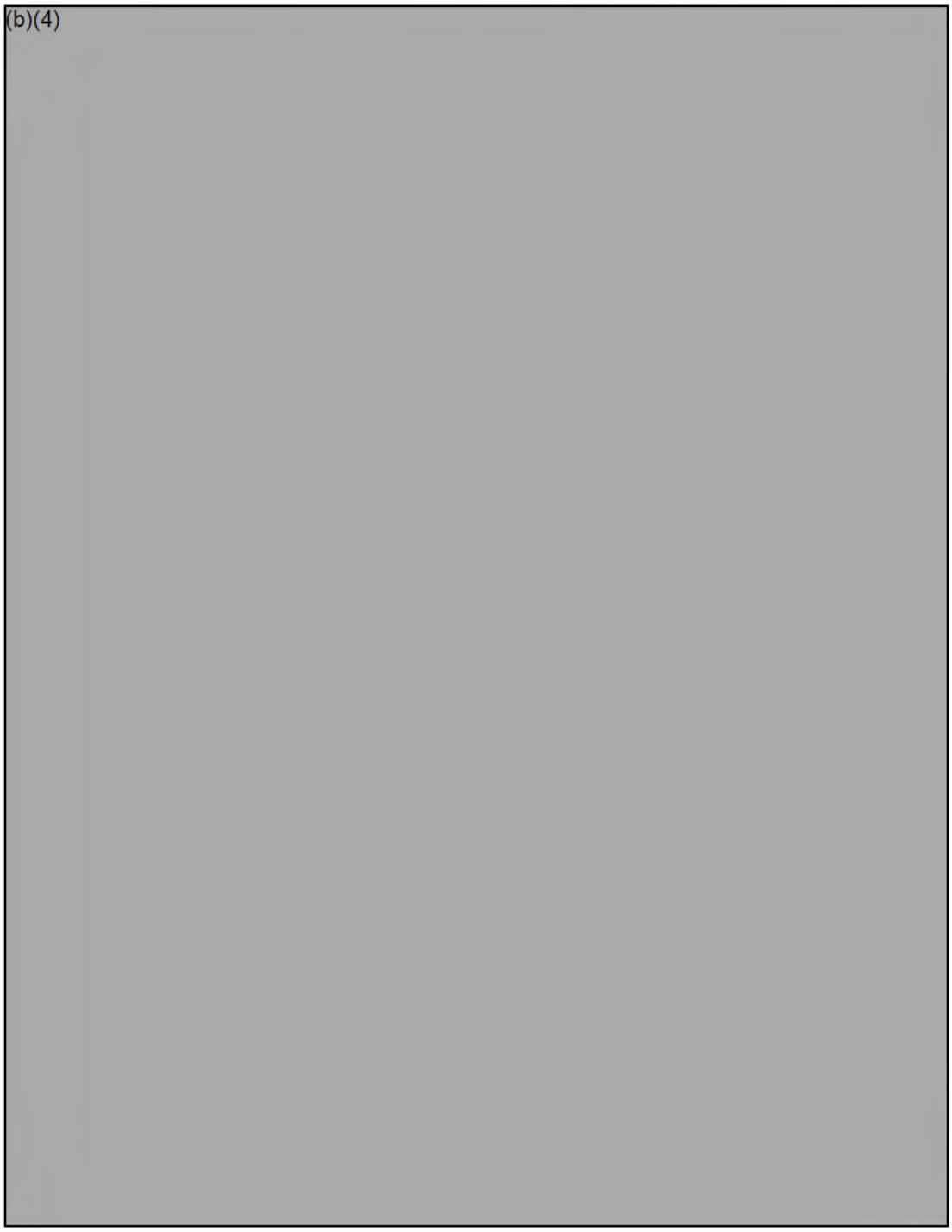

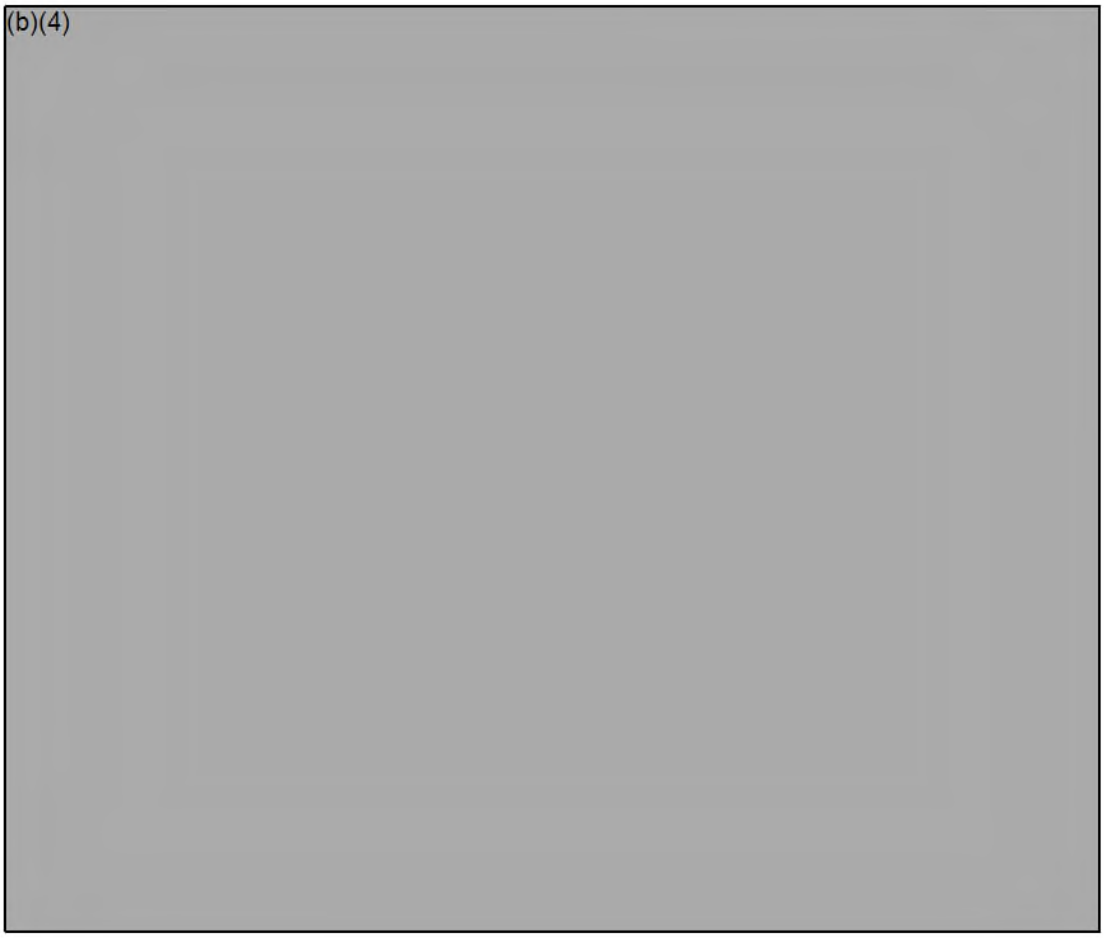

Girth Weld CVN Impact Testing

Sets of longitudinally oriented, 3/4-size CVN specimens were removed from the panels from GW610. In total, three sets of three CVN specimens were notched in the failed joint-side HAZ (FL+1mm), and three sets of three CVN specimens were notched in the weld centerline. Specimens were tested at -5°C. Photographs of the scribed notch locations are included as Appendix G.

(b)(4)

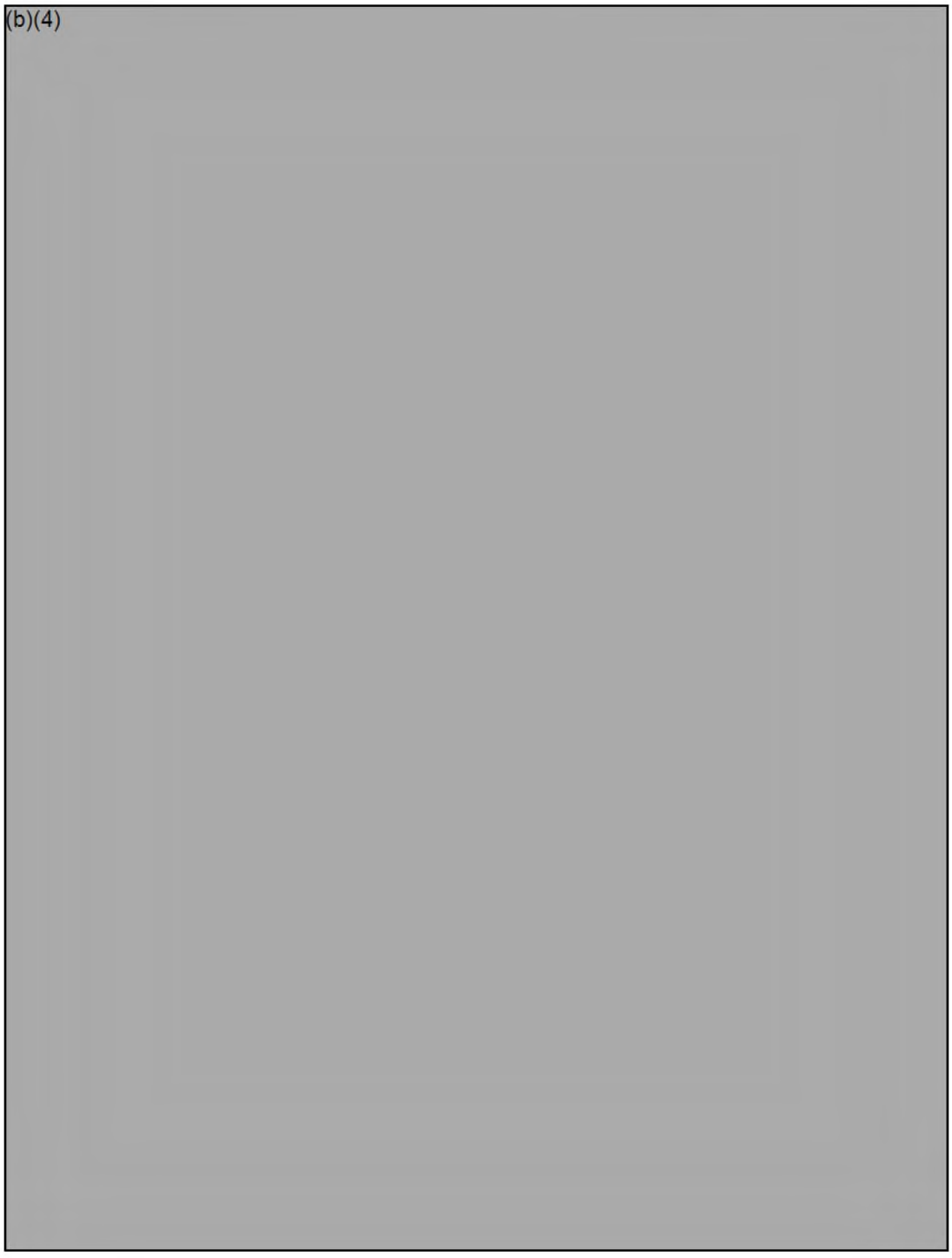

(b)(4)

CTOD Testing

Six, Bx2B SE(B) CTOD specimens were removed from GW610. Three specimens were notched in the failed joint side HAZ, and three were notched in the weld centerline. Photographs showing the notch placement are included as Appendix H. Specimens were removed from locations as nearest to those detailed in the API 1104 20th Ed. A3.2., (b)(4)

(b)(4)

The SE(B) CTOD specimens were compression stress relieved per ISO 15653:2018 Annex C.2. All specimens pre-cracked at room temperature and tested per ISO 15653:2018 at -5°C. The datasheets are included as Appendix I. There were no specifications provided regarding the specified minimum CTOD value for the girth weld, therefore the results are provided for information only. In general, each specimen tested showed no evidence of unstable crack advancement and all went through maximum load, yielding δ_m test results.

GW610			
Specimen	**Zone**	(b)(4)	**Validity**
145-GH1	Pipe HAZ		Valid
145-GH2	Pipe HAZ		Valid
145-GH3	Pipe HAZ		Valid
145-GW1	Weld		Valid
145-GW2	Weld		Valid
145-GW3	Weld		Valid

J-R Fracture Toughness Testing of the Seam Welds and Associated HAZs

Two sets of three, compact tension (C(T)) load-line specimens were removed from the seam weld of each joint; one set from each was notched in the HAZ (FL+1mm) and the other set was notched in the weld centerline. Specimens were tested in accordance with ASTM E1820 at -5°C. The results are summarized in the tables below, the complete J_{IC} toughness report is provided as Annex 1 to this report.

A summary of the data of the HAZ specimens from each joint is shown in Figure 65.

(b)(4)

(b)(4)

Figure 65 *– J-R plots for the* (b)(4)
(b)(4)

Microhardness Testing

A Vickers microhardness survey (HV10) was conducted on metallographically prepared cross-sections. Results were converted to appropriate Rockwell B [HRB] and Rockwell C [HRC] scales per ASTM E140 for ease of interpretation. The results showed no individual test result exceeded the maximum of 280HV prescribed by MPS-BSPC-TC-03[10]. The results of the microhardness tests are provided in Figures 66 – 73.

[10] MPS-BSPC-TC-03 Rev. 1, 9.8.2

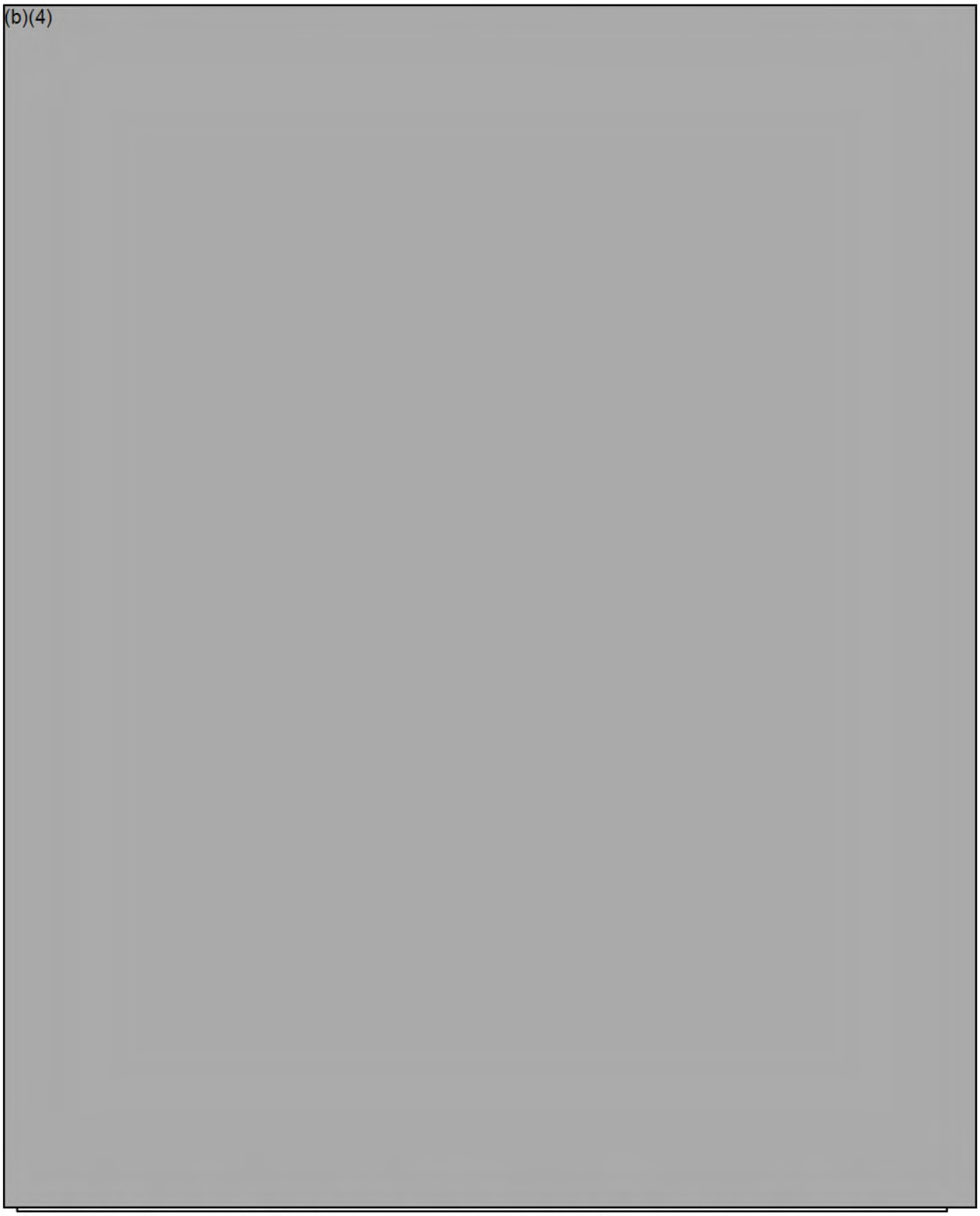

Figure 66 *– Vickers microhardness survey on the upstream joint metallographic section.*

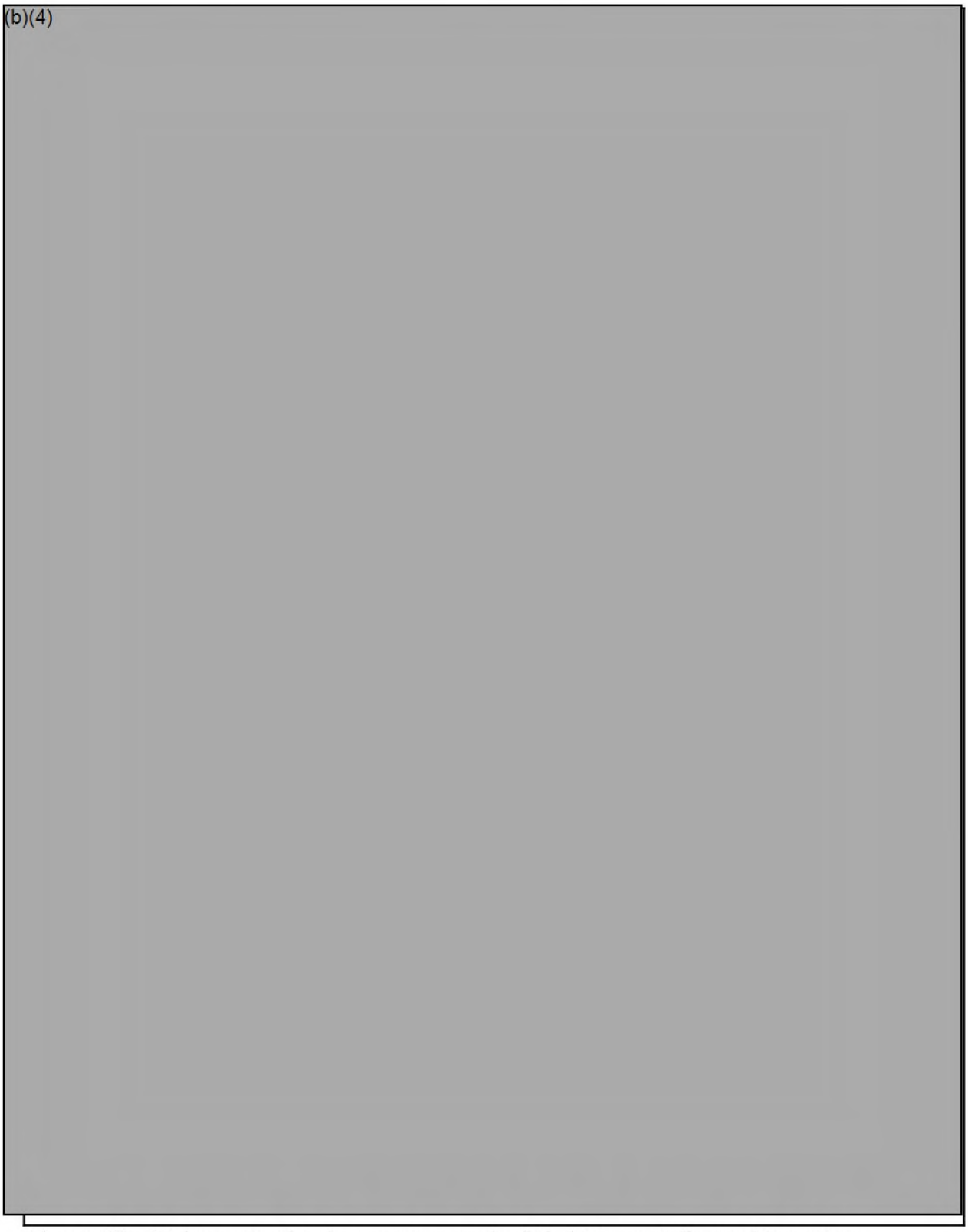

Figure 67 *– Vickers microhardness survey on the failed joint metallographic section.*

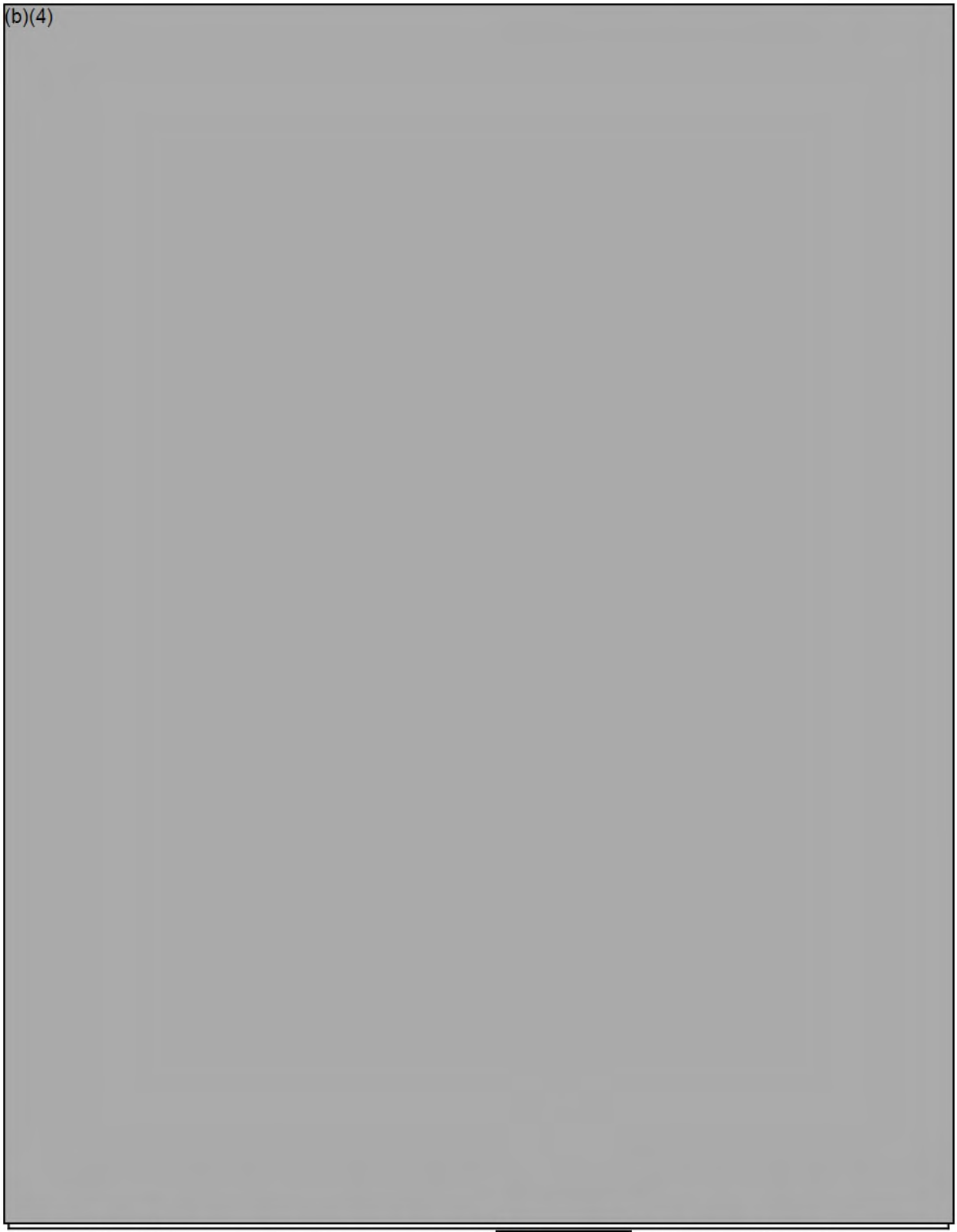

Figure 68 – *Vickers microhardness survey on the* (b)(4) *metallographic section.*

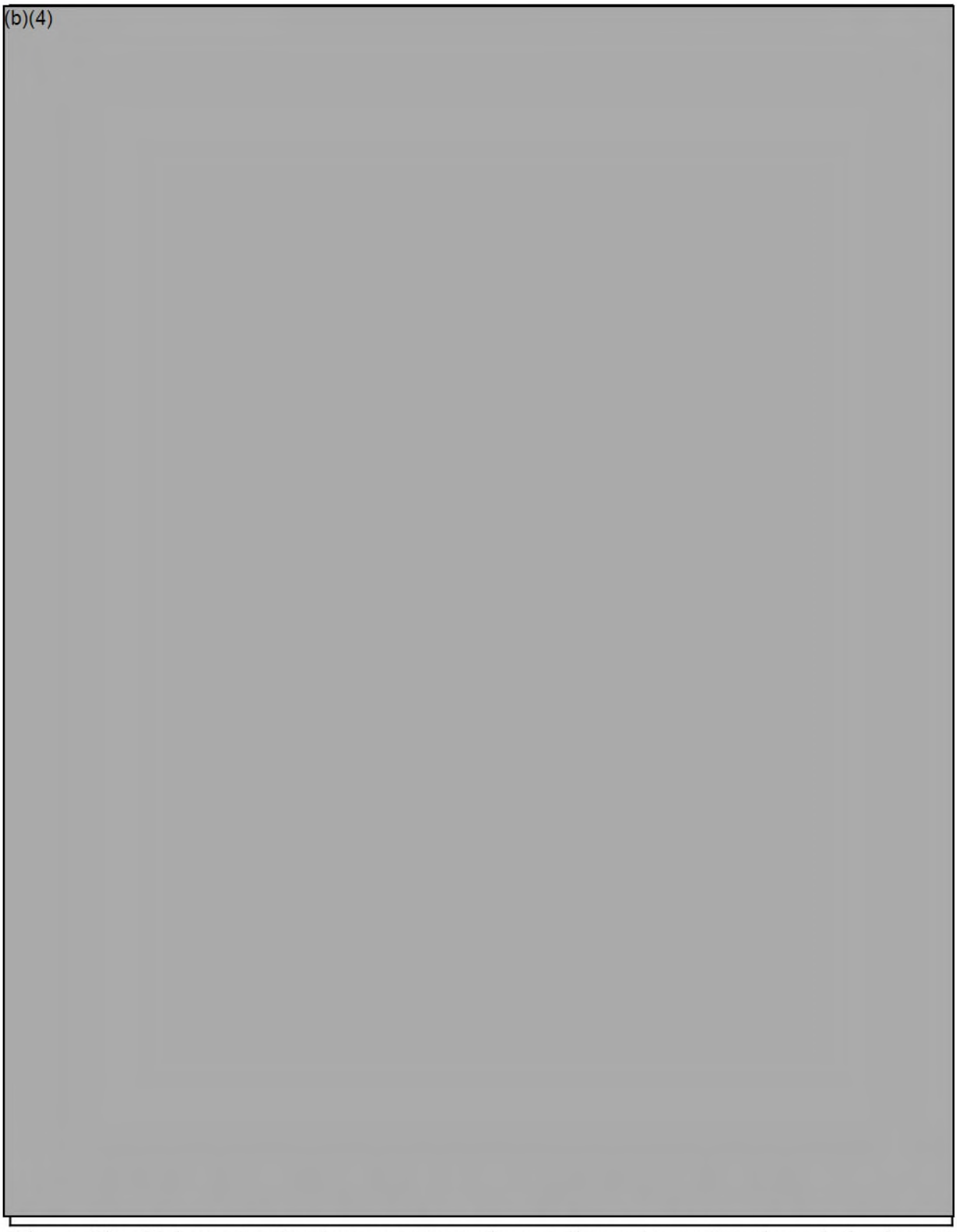

Figure 69 *– Vickers microhardness survey on the metallographic section through the deepest fatigue region.*

Figure 70 *– Vickers microhardness survey on the metallographic section through the 50% wall thickness fatigue region.*

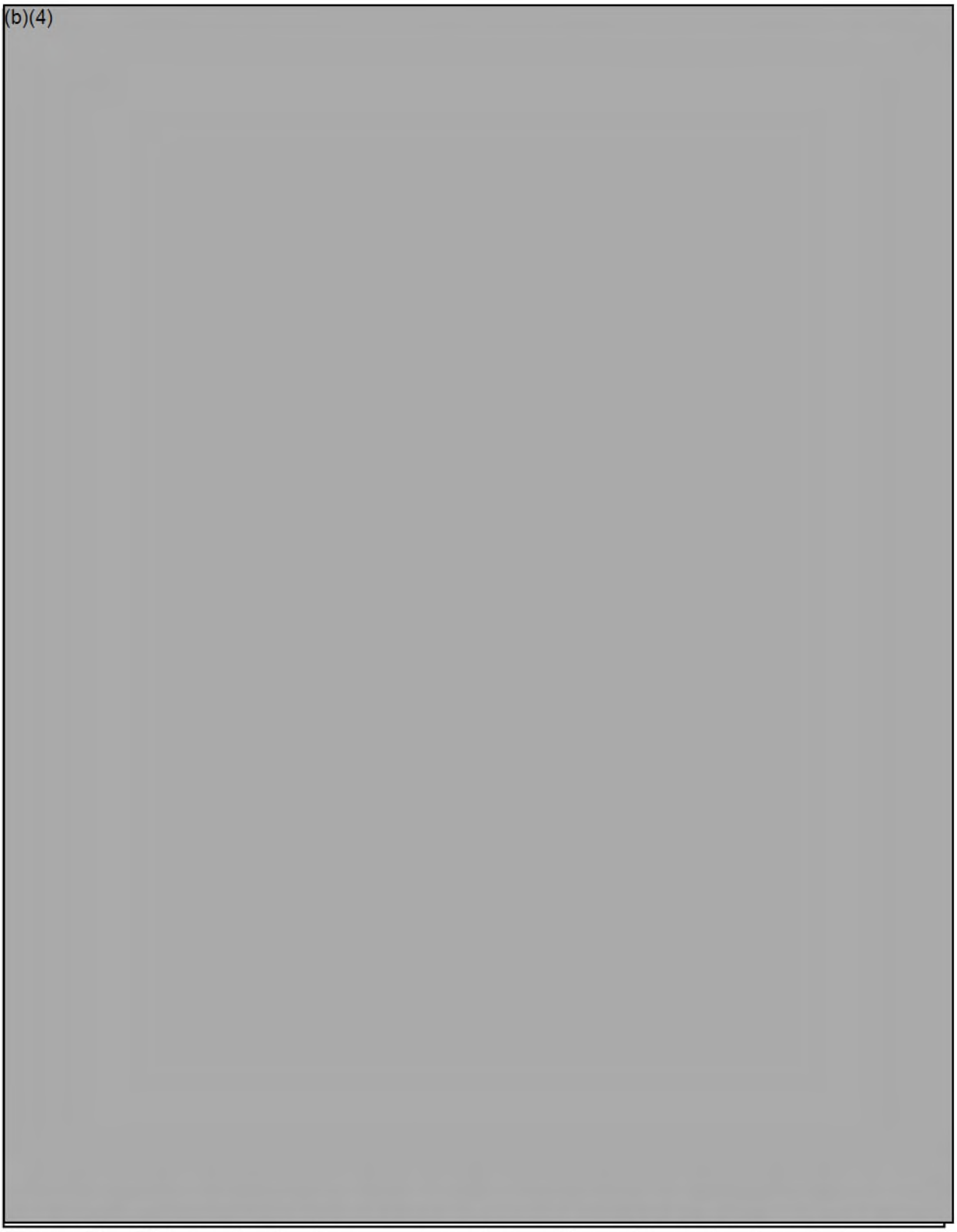

Figure 71 *– Vickers microhardness survey on the metallographic section through the section with 25% wall thickness fatigue.*

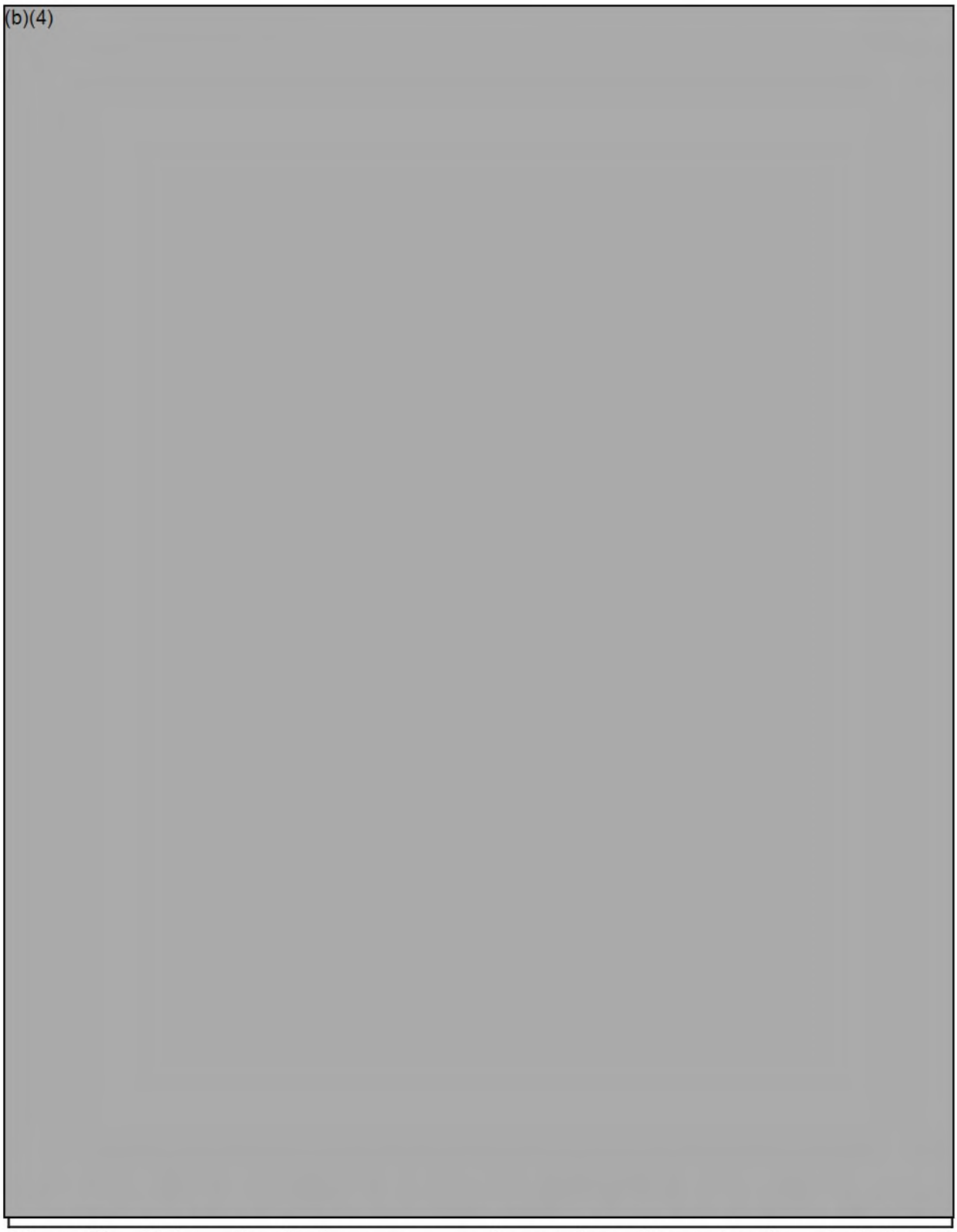

Figure 72 *– Vickers microhardness survey on the metallographic section through shallowest fatigue crack section.*

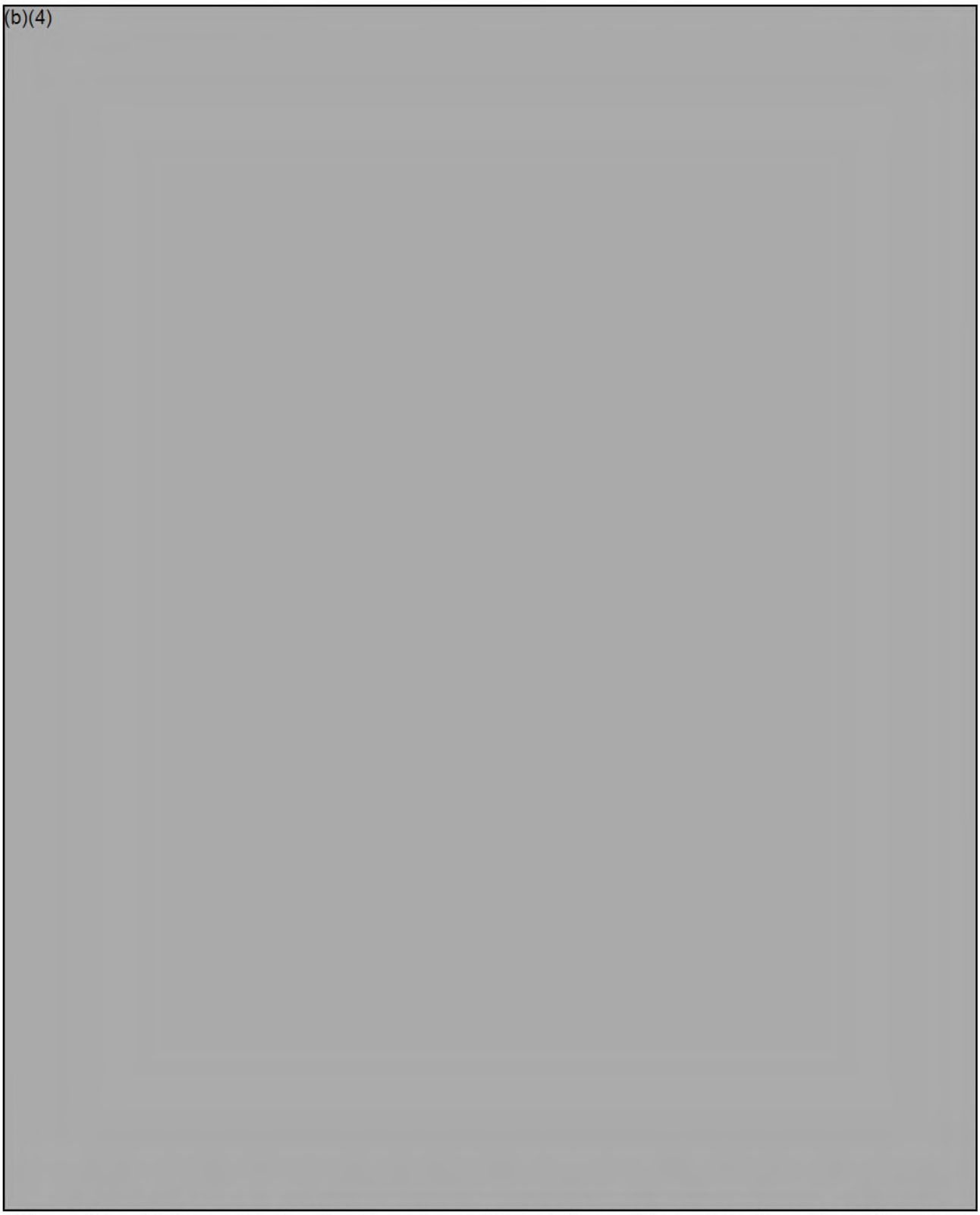

Figure 73 *– Vickers microhardness survey on the metallographic section through shallowest fatigue crack section.*

Chemical Analysis

Coupons from the base metal and seam-weld metal of the upstream, failed, and downstream joints were removed and submitted for a detailed chemical composition determination via optical emission spectroscopy (OES) per ASTM A751. The chemical compositions were compared to the specifications for API 5L grade X70 PSL 2 and MPS-BSPC-TC-03 Rev. 1. The results of the chemical analyses are summarized below. The results of both base metal and weld composition showed no abnormalities or discrepancies with the reported specifications.

(b)(4)

(b)(4)

FINDINGS of FACT

Mechanism of Failure

The cause of the rupture of this section of pipe was attributed to fatigue (progressive) cracking. The fatigue crack initiated at the toe of the seam weld on the ID, centered approximately 1'3.5" upstream of GW610. There was no evidence observed that the fatigue crack penetrated the full wall thickness, indicating the final overload and subsequent petroleum release was an instantaneous event that occurred when the remaining ligament could no longer support the applied load. The orientation of the fatigue cracking being parallel to the seam weld is indicative of hoop stress being a major driving force.

Identified in multiple locations across the ruptured section, and in particular within the fatigued region were small secondary cracks oriented perpendicularly to the fatigue crack. The secondary cracks identified on the fracture surface when examined metallographically showed no evidence of being associated with any microstructural features or inclusions. The secondary cracks also appeared pre-existing to the fatigue crack as the crack arrest lines appeared to be influenced by the presence of these features, specifically in the sense that the arrest lines appeared to bend around the cracks. The secondary cracks were predominantly transgranular, free of any residual scale, and were located in the fine-grained, equiaxed HAZ region. These findings suggest the possibility of the secondary cracks as being associated with a hydrogen cracking mechanism.

Conformance of Pipe with Respect to API 5L, 43rd Ed.

There was no evidence found to support a finding that the pipe was materially or structurally deficient with respect to the requirements of API 5L, 43rd Ed. The mechanical properties and chemical composition of the pipe met the minimum specifications for API 5L grade X70 PSL 2.

Conformance of Pipe with Respect to MPS-BSPC-TC-03, Rev. 1

A full review of pipe conformance with MPS-BSPC-TC-03, Rev. 1 was not within the scope of the metallurgical examination. Testing data collected during the course of this investigation

shows the chemical properties and mechanical properties (tensile and impact) to be within the specified limits in the specification.

Weld Geometry

Geometric measurements of metallographic sections across the seam welds of the failed joint, upstream joint, and downstream joint showed each would be within the specified limits of radial misalignment[11], out-of-line weld bead[12], and cap height[13] set forth in API 5L 43rd Ed. There was approximately 3.7mm of offset of the ID/OD seam weld centerlines on the failed joint, which conforms to the requirements of the 43rd Ed in that this offset is not cause for rejection provided complete penetration and fusion has been achieved.

Angular measurements were acquired for the purpose of subsequent evaluation for peaking/roof topping. A determination pertaining to the contribution, if any, to any peaking/roof topping effect was outside the scope of this metallurgical analysis.

DISCUSSION and CONCLUSIONS

Fatigue, under most loading conditions is considered a sub-critical cracking mechanism, meaning it progresses at stresses below the yield strength and propagates without any appreciable plastic deformation, particularly in the Stage II region. Consequently, fatigue cracking often appears macroscopically brittle, and only at high magnifications can the striations demarcating incremental crack growth can be observed. (b)(4)

(b)(4)

[11] API 5L, 43rd Ed., 7.8.2
[12] API 5L, 43rd Ed., 7.8.3
[13] API 5L, 43rd Ed., 7.8.4

As a method to eliminate possible imaging conditions (accelerating voltage and spot size) biasing the fracture surface analysis, the fatigued region was examined using varying combinations of each variable. The results were consistent in that evidence satisfying a finding that striations were present on the surface was not observed. Consideration was also given to the possibility that post-fracture surface degradation had obscured striations; this possibility was eliminated primarily due to the lack of evidence of post-failure corrosive attack and the findings that cleavage features appeared crisp.

The incremental brittle advancement of the fatigue crack was further substantiated via J-R fracture toughness testing, (b)(4) (b)(4) (b)(4) A study published by NIST in 2024[14] reported nearly identical findings in terms of the behavior of the heat affected zone toughness in quasi-static loading. The authors of the study also report similar findings regarding impact toughness behavior of the weld and HAZ regions, with impact toughness values of the HAZ being comparable to the base metal, while the specimens notched in the weld were less tough.

The progression of the fatigue crack appears to have occurred through a series of incrementally unstable crack advancements and self-arrests. Absent any metallurgical anomalies in the failed region, a possible explanation for the brittle nature of the failure is a hydrogen mechanism. Evidence supporting this as a possible contributing factor aside from the brittle appearance of the fracture was the secondary cracking that appeared consistent with HIC cracking. HIC cracks form via absorption of atomic hydrogen, and form preferentially at locations in the microstructure where the atomic hydrogen become "trapped". Common trapping sites for hydrogen in a steel microstructure include non-metallic inclusions, grain boundaries, and carbide banding. To re-iterate, there was no evidence of anomalous microstructural conditions or

[14] Newell Moser, et al., "Hydrogen Embrittlement Susceptibility and Fracture Toughness Measurements of Welded X65M Pipeline Steels". Proceedings of ASME 2024, Pressure Vessels & Piping Conference. July 29 – Aug. 2, 2024, Bellevue, WA.

inclusions identified in the region surrounding the rupture. With enough accumulation of hydrogen in the trap sites, the hydrogen can recombine into molecular (gaseous hydrogen) resulting in a crack that is typically parallel to the rolling direction of a steel plate.

There are several possible sources of hydrogen absorption, but none are verifiable by this metallurgical examination. Some possible, though non-exhaustive sources of hydrogen impregnation include corrosion, especially in wet hydrogen sulfide environments, excessive cathodic protection (cathodic hydrogen charging), and welding. Welds and their associated heat affected zones are generally more susceptible than base metal or non-welded material due to factors including variations in residual stresses, geometric stress concentration, and variations in chemistry between the weld and base metal.

In summary, the rupture of this pipe was attributed to fatigue originating along the ID toe of the seam weld. There was evidence of micropitting observed, and some of the micropits acted as crack initiation sites. The results of the mechanical testing regiment showed no deficiencies with respect to either API 5L, 43rd Edition or MPS-BSPC-TC-03 Rev. 1. The propagation mode of the fatigue crack appeared consistent with incremental brittle crack advancement. The cause of the brittle nature of the crack advancement appears to be associated with a hydrogen mechanism.

If you have any questions, or need any additional information, please let us know. The samples from this investigation will be held for a period of 30 days following the completion of the RCFA. Long-term storage of the material involved in this investigation should be transferred to a firm that specializes in categorizing and storing evidence in potential litigation cases.

Respectfully submitted June 13, 2025.

ANDERSON & ASSOCIATES, INC.
Engineering Firm Registration # F-816

(b)(6)